

Ms# 201411001R

**Rme-8 depletion perturbs Notch recycling and predisposes to pathogenic signalling**

**Maria J Gomez-Lamarca<sup>1,3</sup>, Laura A. Snowdon<sup>1,3</sup>, Ekatarina Seib<sup>2</sup>, Thomas Klein<sup>2</sup> and Sarah J Bray<sup>1\*</sup>**

1: Department of Physiology Development and Neuroscience

University of Cambridge

Downing Street

Cambridge, CB2 3DY

2: Institute of Genetics

Heinrich-Heine-Universität Düsseldorf

Universitätsstr. 1

40225 Düsseldorf

3: authors contributed equally to this work

**\* Author for correspondence**

**[sjb32@cam.ac.uk](mailto:sjb32@cam.ac.uk)**

**+44 1223 765222**

**Running title:** Notch recycling requires Rme-8

**e-TOC Summary Statement:** The retromer-associated DNAJ protein Rme-8 is necessary for normal Notch recycling, and reductions in Rme-8 sensitize cells so that additional loss of sorting retromer or ESCRT-0 components has catastrophic effects.

**Key words:** Rme-8, Notch, Rab4, endocytosis, receptor recycling

**Character count:** 41,954

## ABSTRACT

Notch signalling is a major regulator of cell fate, proliferation and differentiation. Like other signalling pathways its activity is strongly influenced by intracellular trafficking. Besides contributing to signal activation and down-regulation, differential fluxes between trafficking routes can cause aberrant Notch pathway activation. Investigating the function of the retromer-associated DNAJ protein Rme-8, *in vivo*, we demonstrate a critical role in regulating Notch receptor recycling. In the absence of Rme-8, Notch accumulated in enlarged tubulated Rab4-positive endosomes and, as a consequence, signalling was compromised. Strikingly, when the retromer component *Vps26* was depleted at the same time, Notch no longer accumulated and instead was ectopically activated. Likewise, depletion of ESCRT-0 components *Hrs* or *Stam* in combination with *Rme-8* also led to high levels of ectopic Notch activity. Together these results highlight the importance of Rme-8 in co-ordinating normal endocytic recycling route and reveal that its absence predisposes towards conditions where pathological Notch signalling can occur.

## INTRODUCTION

The highly conserved Notch signalling pathway is a key regulator of many developmental decisions, controlling processes such as proliferation and differentiation. Inappropriate pathway activation is associated with several human diseases, including hematopoietic and solid tumors (Lobry et al., 2011). As a consequence, tight spatiotemporal regulation of Notch activity is essential. Intracellular trafficking is an important element in such regulation, influencing steps involved in signal activation as well as in preventing inappropriate signalling (Brou, 2009).

In canonical signalling, Notch is activated by ligands of the Delta, Serrate, Lag-2 (DSL) family presented by neighbouring cells. Upon ligand-binding, Notch undergoes two consecutive proteolytic cleavages, catalyzed by an ADAM metalloprotease (S2 cleavage) and the  $\gamma$ -secretase complex (S3 cleavage). The latter releases the Notch intracellular domain (NICD) from the membrane, which translocates to the nucleus, where it regulates transcription of a variety of target genes (Bray, 2006). Signalling is highly sensitive to levels, localization and modifications of the membrane proteins, which in turn are dependent on vesicular trafficking routes. For example, regulated trafficking is important for active ligand function and for turnover of inactive Notch receptors (Brou, 2009). In addition, ligand-independent trafficking of the full-length receptor to the late endosome and lysosome can result in activation (Fortini and Bilder, 2009). In *Drosophila*, the ring finger protein Deltex is one factor that promotes signalling via this alternate late-endosomal mechanism, which, like ligand induced activation, relies on  $\gamma$ -secretase mediated cleavage (Baron, 2012).

For endocytosed cargoes to reach the correct final destination, they have to be sorted into distinct endosomal compartments (e.g. SupFig 3L). A significant fraction of endocytosed Notch is transferred into intraluminal vesicles (ILVs) of so-called Multi-Vesicular Bodies (MVB), destined for degradation once MVBs fuse with lysosomes (Henne et al., 2011). The sorting and internalization of cargoes into ILVs is carried out by Endosomal Sorting Required for Transport (ESCRT) complexes. Mutations affecting this process result in Notch being retained in the limiting membrane of MVBs where conditions facilitate proteolytic release of NICD, resulting in ectopic signalling (Hori et al., 2011; Moberg et al., 2005; Thompson et al., 2005; Vaccari and Bilder, 2005; Vaccari et al., 2008)

Besides being routed to lysosomes for degradation, internalized proteins can be recycled back to the plasma membrane or transferred to the Golgi. Early endosomes, marked by Rab5 GTPase, are the hub where internalized cargoes are sorted into different domains depending on their destination. For example, Rab4 marks a tubular sub-domain of early endosomes that is involved in rapid recycling of cargoes to the plasma membrane. Cargoes destined for recycling are concentrated in tubular extensions through the actions of complexes, including retromer (Jovic et al., 2010). First identified due to its role in retrograde transport from early endosomes to Trans-Golgi, retromer is also involved in direct endosome-to-plasma membrane transport of proteins like the  $\beta$ 2-adrenergic receptor (Seaman, 2012; Seaman et al., 2013). It consists of two sub-complexes, a cargo-sorting sub-complex, composed of Vps35/Vps26/Vps29, and a sorting nexin sub-complex (SNX), which promotes tubulation (McGough and Cullen, 2011). The associated proteins include the DNAJ protein Receptor-Mediated Endocytosis-8 (Rme-8), whose absence leads to highly branched endosomal tubules and mis-sorting of cargoes (Freeman et al., 2014; Popoff

et al., 2009; Shi et al., 2009). Indeed, pathogenic mutations in *Rme-8* and in *Vps35* have been found in some instances of familial Parkinson's disease, underscoring the importance of endosomal recycling pathways (Vilarino-Guell et al., 2014; Vilariño-Güell et al., 2011).

First identified as a protein required for endocytosis in *Caenorhabditis elegans* (Girard et al., 2005), evidence now indicates that Rme-8 is primarily involved in post-endocytic transport steps. While the Hsc40-binding DNAJ-domain is the only obvious feature of its sequence, biochemical studies have shown that the mammalian protein can bind to retromer components (SNX1) and WASH complex through other parts of the protein (Freeman et al., 2014; Popoff et al., 2009; Shi et al., 2009). Rme-8 may therefore link together requisite elements of the transport machinery in endocytic tubules (Freeman et al., 2014), but it remains to be established what role the DNAJ-domain or Hsc40 play in this process.

Although previous studies have not detected a requirement for retromer in normal Notch function (Belenkaya et al., 2008; Franch-Marro et al., 2008; Pocha et al., 2011), our small scale screen for factors influencing Notch, along with larger screens by others (Le Bras et al., 2012), identified *Rme-8* as a potential regulator. Therefore we have investigated here the role of Rme-8 in Notch trafficking and in the organization of the endosomal network *in vivo*. Our results indicate that Rme-8 is necessary for normal Notch recycling. Furthermore, they reveal that reductions in *Rme-8* sensitize the cells so that additional loss of sorting retromer or ESCRT-0 components has catastrophic effects. The fact that such synthetic combinations result in ectopic Notch activity and tissue overgrowth has major implications in the context of human disease-mutations affecting *Rme-8* and related genes.

## RESULTS

### **Rme-8 is a positive regulator of the Notch pathway**

In a small-scale genetic screen, using an *RNAi* (*Ri*) collection against known trafficking proteins, we identified the DNAJ protein Rme-8 as a positive modulator of the Notch pathway. *Rme-8* knockdown at late stages of wing development (using *Sal<sup>EPv</sup>-Gal4* to express *Rme-8 Ri*; **Fig 1A**; Cruz et al., 2009) gave rise to wings with thickened veins (L2, L3) and, occasionally, small deltas (arrows, **Fig 1C**). This phenotype is reminiscent of reduced Notch function as illustrated by phenotypes produced when the Notch pathway transcription factor, Su(H), was perturbed using the same conditions (**Fig 1D**). Additional defects, such as posterior vein loss and more severe changes in wing morphology were also observed, indicating that Rme-8 has Notch-independent roles (arrowhead, **Fig 1C**). However, the penetrance of the vein thickening phenotypes suggests that the Notch pathway may be particularly sensitive to *Rme-8* depletion.

To verify that *Rme-8* depletion affected Notch activity, we assessed the consequences on a Notch Responsive Element (NRE) reporter, *NRE-mCherry*, when *Rme-8-Ri* was expressed in the posterior domain of wing imaginal discs (using *engrailed(en)-Gal4*; **Fig 1E**). Normally NRE-mCherry is strongly expressed in a stripe along the dorso-ventral (D/V) boundary with lower levels in flanking inter-vein regions (Housden et al., 2012; **Fig. 1F**). Knockdown of *Rme-8* (**Sup Fig 1A**) led to reduced NRE-mCherry expression, both at the D/V boundary and in surrounding regions (**Fig 1G,J**), although to a substantially lesser extent than depletion of *Su(H)* in the same way (**Fig 1H**). In these (and subsequent experiments) similar phenotypes were obtained using two independent RNAi lines that target different regions in *Rme-8* transcripts (*Rme-8<sup>KK</sup> Ri*

and *Rme-8<sup>GD</sup> Ri*, the former gave slightly stronger phenotypes). Likewise, *NRE-mCherry* expression was reduced in clones of *Rme-8* mutant cells, generated with a previously described X-ray induced loss-of-function allele (*Rme-8<sup>C19</sup>*, Chang et al., 2004; **Fig 1I,J**). Together, these data indicate that *Rme-8* is required for full Notch pathway activity and that it normally acts as a positive regulator of Notch function.

### **Aberrant Notch and Wingless localization in the absence of *Rme-8*.**

Since *Rme-8* is an evolutionary conserved endosomal-associated protein (Chang et al., 2004; Fujibayashi et al., 2008; Girard and McPherson, 2008; Girard et al., 2005; Popoff et al., 2009; Shi et al., 2009; Zhang et al., 2001), it likely affects Notch signalling by altering trafficking of key pathway components. We therefore investigated the consequences of *Rme-8* knockdown on the distribution of Notch and its ligand, Delta (Dl). Both proteins accumulated together in enlarged intracellular puncta in *Rme-8* depleted territories (arrowheads, **Fig 2A**), demonstrating that *Rme-8* is required for proper Notch and Dl trafficking. Concomitant with the increase in intracellular accumulation, their levels at the plasma membrane were decreased (**Fig 2A-D; SupFig 1B**). Furthermore, the intracellular puncta contained both intracellular (NICD) and extracellular domains of Notch (NECD), suggesting that the un-cleaved form of the receptor accumulates upon *Rme-8* depletion (arrowheads, **Fig 2B-B''**). Similar intracellular Notch puncta were also present in *Rme-8* mutant cells (*Rme-8<sup>C19</sup>*, **Fig 2E**; *Rme-8<sup>A9</sup>*, **SupFig 1C**). Although both Notch and Dl were affected, the reduced signalling appeared autonomous to *Rme-8* depleted cells, suggesting that the receptor is particularly compromised (rather than the ligand). Phenotypes in the ovary also indicated a requirement for *Rme-8* in signal receiving follicle cells rather than the signal-sending oocyte (data not shown) arguing that the primary defect arises from changes to Notch function.

Although adult phenotypes were reminiscent of Notch loss of function, Rme-8 is likely to have broader effects on endocytosis. In agreement, Wingless (Wg) distribution was also altered in *Rme-8* depleted discs. Notably, Wg was detected at a broad range from its site of synthesis (**Fig 2F**) and accumulated within cells at a distance from the Wg producing cells (**SupFig 1D**). These consequences were similar to those reported for *Hrs* loss of function (Piddini, 2005; Rives et al., 2006) and suggest that Wg trafficking within receiving cells becomes compromised when *Rme-8* is depleted. In contrast, Wg secretion appeared relatively normal. Firstly, the distribution of extracellular Wg in *Rme-8* depleted tissue was similar to wild-type (WT; **SupFig 1E**). Second, *senseless*, a gene whose expression requires high levels of Wg signalling (Nolo et al., 2000) was still expressed in *Rme-8* depleted cells (**SupFig 1F-G**). These data argue that Wg secretion, which relies on retrograde recycling of its chaperone, Wntless, via a retromer dependent route to the Golgi (Belenkaya et al., 2008; Franch-Marro et al., 2008; Harterink et al., 2011; PAN et al., 2008; Port et al., 2008; YANG et al., 2008; Zhang et al., 2011), was still functional in *Rme-8* depleted cells although other aspects of Wg trafficking were perturbed. As the adult phenotypes from *Rme-8* depletion are however most allied to deficits in Notch signalling, subsequent analysis was focused on the consequences on Notch trafficking and function.

### **Rme-8 regulates Notch trafficking**

One strategy to investigate the stage at which trafficking is arrested is to follow the uptake of receptor-bound antibodies in live tissues (Le Borgne and Schweisguth, 2003). Using an antibody against NECD we tracked the intracellular route by monitoring the location of antibody-Notch complexes at different times after the unbound antibody was washed out. First we established mild conditions of *Rme-8*

knockdown, so that, at time 0, there were similar levels of  $\alpha$ -NECD antibody bound at the cell surface in control and *Rme-8* depleted compartments (**Fig 3A, D, I**). We then transferred tissues to RT and analysed changes in distribution.

After 30min internalization, large amounts of Notch-antibody complex were already accumulated in sub-apical puncta in *Rme-8* depleted regions (**Fig 3B, E, G, H**). After 2 hr, these sub-apical puncta were more pronounced (**Fig 3C',F,G H**) and the amount of Notch-antibody complex at the cell surface was reduced in comparison to neighbouring WT tissue (**Fig 3C, I**). At this time, the internalized complexes in WT tissue were enriched basally (**Fig 3C'', F**) and most likely corresponded to a pre-lysosomal compartment. The results therefore demonstrate that Notch is internalized in *Rme-8* depleted tissue and accumulates in an apical compartment. In support, accumulation of Notch was prevented by combined knock down of *Rme-8* with *avalanche* (**Sup Fig 3H**), which is required at the earliest stages of endocytic trafficking (Lu and Bilder, 2005). The decrease in antibody-associated Notch at the membrane at 30min and 2h (**Fig. 3I**) suggests either that Notch is endocytosed more rapidly in the absence of *Rme-8* or that there is a defect in recycling of Notch back to the plasma membrane following endocytosis. Given the previously observed association of *Rme-8* with endosomes (Chang et al., 2004; Freeman et al., 2014), the latter seems more likely.

Notch trafficking is regulated by E3-ubiquitin ligases including Deltex (Dx) and Suppressor of Deltex [Su(dx)] (Hori et al., 2004; Wilkin et al., 2004; Yamada et al., 2011). For example, overexpression of Dx modifies the destination of Notch, causing ectopic activation detectable by ectopic NRE-GFP expression and tissue overgrowth (**SupFig 2A**; Hori et al., 2004; Yamada et al., 2011). However, neither ectopic Notch

activation nor overgrowth phenotypes were reduced when *Rme-8* was depleted in Dx-overexpressing discs (**SupFig 2B**) suggesting they operate on different trafficking routes. In addition, Notch accumulations were detected throughout the cell, not just sub-apically as in *Rme-8* knockdown (**SupFig 2C-F**). In converse experiments, Dx knockdown led to membrane accumulation of Notch whereas the phenotype in combination with *Rme-8-Ri* appeared to be an aggregate (**SupFig 2E-L**). Likewise, similar experiments combining *Rme-8-Ri* with Su(dx) over-expression also yielded an aggregate of phenotypes (**SupFig 2M-P**). Together, these results suggest that the pools of Notch modified by Dx and Su(dx) are likely to be separate from those trapped by *Rme-8* knockdown.

### **Rme-8 depletion results in enlarged endosomes, where Notch accumulates in proximity to Rab4, and alters Notch dynamics at the membrane**

To investigate where in the endocytic network Notch accumulated when *Rme-8* was depleted, tissues were co-stained for Notch and endosomal markers (Summarized in **SupFig 3G,L**). First, Rab5 puncta showed little change in *Rme-8* deficient cells, indicating that early endosomes form normally, and relatively few Rab5 puncta were associated with Notch (**SupFig 3A**). Second, markers of maturing endosomes, Rab7 and Hrs, were present in larger aggregates than in WT (**Fig 4A, SupFig 3B**) that were found in proximity to large Notch accumulations, although there was limited co-localization. Third, Notch puncta were also labelled by the PI(3)P sensor FYVE-GFP and by the FYVE-domain containing protein SARA (Smad anchor for receptor activation), indicating that Rab5 mediated recruitment of phosphatidylinositol-3-kinase had occurred (**SupFig 3C, E**). The size of SARA puncta was also increased. Finally, the endolysosomal protein, Lamp1, was detected in enlarged structures, although showed relatively low co-localization with Notch (**SupFig 3F**). These results

indicate that loss of *Rme-8* affects maturing endosomes and that, although Notch is associated with these, it is primarily confined to a domain distinct from those marked by Hrs or Rab7 (**SupFig 3L**).

Other endosomal subdomains include those involved in Rab4 and Rab11 dependent recycling to the plasma membrane (Grant and Donaldson, 2009; Li et al., 2008; Sönnichsen et al., 2000). As with other markers, *Rme-8* depletion resulted in enlarged Rab4 and Rab11 puncta, which largely segregated into distinct domains (**Fig 4B**). The most marked effect was with Rab4, which also exhibited the most intimate relationship with Notch (**Fig 4A,B**). The retromer Vps26 subunit showed a similar co-localization (**SupFig 3D**). Altogether the results support a model where the absence of *Rme-8* generates maturing endosomes that are comprised of an array of enlarged subdomains. The preferential relationship between Notch, Rab4 and Vps26 in this enlarged structure, suggests that the receptor is trapped in a recycling compartment (**SupFig 3L**).

Using 3D-structured illumination microscopy it was possible to further resolve the endosomal structures containing Notch. In WT cells, Notch associated with Rab4 labelled endosomal structures with a perimeter of  $\sim 2.5\text{-}3.5\mu\text{m}$  (**Fig 4C**). Elongated Rab4 and/or Notch labelled structures extended out from and across each endosome, consistent with them forming part of the tubular endosomal network (e.g. **arrow, Fig 4C**). Punctate Rab7 was normally segregated into an adjacent domain, although occasionally Rab7 and Notch puncta were directly juxtaposed (**arrowheads, Fig 4E**). After *Rme-8* depletion, Notch and Rab4 were present in enlarged structures approximately  $4\text{-}6\mu\text{m}$  in perimeter (**Fig 4D**). A punctuated circumferential ring of Rab4 was usually evident, but was larger in *Rme-8* depleted tissues and the

protrusions, likely tubules, were more extensive (**Fig 4D,G**). Alternating segments of Rab4 and Notch were detected in several of these, suggesting they are present in the same protrusions (**arrow, Fig 4D**). Rab7 was also associated with the same large structures, but was largely segregated from Notch (**arrowheads, Fig 4F**). Altogether, these results indicate that Notch accumulates preferentially in Rab4 positive compartments, and show that the endosomes detected following *Rme-8* depletion are enlarged with more extensive tubule-like structures than in WT. A similar increase in highly branched endosomal tubules occurred in *Rme-8* depleted HeLa cells (Freeman et al., 2014).

Enlarged maturing endosomes were also detected by transmission electron microscopy (TEM) (**Fig 4H-J and SupFig 4**). Sectioning the discs to directly compare WT and *Rme-8*-depleted tissue, showed that the mean size of MVBs (identified by the presence of ILVs) was 2-3x greater than in WT (**Fig 4J and SupFig 4D, H-I**). While the TEM did not capture the tubular morphology suggested by the super-resolution images, the size of the structures observed was similar using the two methods (2.5-4 $\mu$ m perimeter). Thus it appears that in the absence of *Rme-8*, the vacuolar endosome and associated tubular network become greatly enlarged.

The localization studies show that a significant proportion of Notch associates with Rab4 when *Rme-8* is reduced. One explanation is that *Rme-8* is necessary for normal recycling of Notch, and that, when *Rme-8* is missing, Notch is trapped in a recycling domain of the sorting endosome. To investigate further, we monitored the dynamics of Notch protein at the membrane via Fluorescence Recovery After Photo-bleaching (FRAP) (**Fig 4K-L**) using a functional Notch-GFP fusion protein (Couturier et al., 2012). Small circular regions along apical cellular junctions were bleached, (red circle, Fig

4L) and the re-appearance of unbleached Notch-GFP measured in WT and *Rme-8* depleted cells. The recovery with time was significantly altered in *Rme-8* depleted cells compared to wild-type controls (**Fig 4K**). These data demonstrate that the dynamics of Notch proteins at the membrane are reduced. Furthermore, the Notch-GFP recovery was also curtailed by treating the tissues with the dynamin inhibitor dynasore, indicating that endocytic trafficking contributes to the recovery (Supp Fig. 3I,J). However, these results do not unequivocally demonstrate that recycling is affected in the *Rme-8* depleted cells as several factors can contribute to recovery and the experiments are not able to distinguish direct from indirect effects. Nevertheless, as Notch becomes trapped with Rab4 and Vps26 in the *Rme-8* depleted cells, it is likely that the reduced recovery of Notch-GFP reflects, in part, a defect in endocytosis-mediated recycling

### **Combined knockdown of Vps26 and Rme-8 leads to ectopic Notch activity**

Many recycling pathways involve the retromer complex, including the Rab4-associated route to the plasma membrane (Seaman, 2012; Seaman et al., 2013; Steinberg et al., 2013; Temkin et al., 2011; Wang et al., 2014). Furthermore, *Rme-8* localizes at places where retromer-mediated sorting occurs (Freeman et al., 2014; Popoff et al., 2009; Shi et al., 2009). To investigate whether Notch trafficking defects in *Rme-8* depleted cells involve retromer, we analysed the consequences from depleting *Vps26*.

First, we monitored consequences on *NRE-mCherry* when *Vps26* was depleted either alone or together with *Rme-8*. *Vps26* single knockdown had little impact on *NRE-mCherry* expression (**Fig 5A**), indicating that Notch activity was not substantially changed by retromer depletion as reported previously (Franch-Marro et al., 2008).

Strikingly however, the combined knockdown of *Vps26+Rme-8* resulted in NRE expression throughout the domain, indicating that this combination results in strong ectopic Notch activation (**Fig 5B**). The reduced Vps26 protein levels (**Sup Fig. S5A**) along with the accumulation of Wg (**Fig 5C**), whose secretion depends on retrograde transport of Wntless in a retromer-dependent manner, confirmed the efficacy of *Vps26* knockdown (Belenkaya et al., 2008; Franch-Marro et al., 2008; Harterink et al., 2011; PAN et al., 2008; Port et al., 2008; YANG et al., 2008; Zhang et al., 2011). The slight broadening of Wg expression in *Vps26+Rme-8* combined knockdowns is consistent with the ectopic *NRE-mCherry* expression in this genotype, (**Fig 5D**) since *wg* is a Notch target. Mutations affecting a second component of the retromer complex, *Vps35*, had a similar effect to *Vps26<sup>Ri</sup>*. Thus *Rme-8* knockdown in *Vps35* mutant cells resulted in ectopic expression of *deadpan*, a HES gene directly regulated by Notch in this tissue (**Sup Fig 5B-D**).

In agreement with the minimal effects on *NRE-mCherry* expression, there was little consequence on Notch intracellular distribution or Notch membrane levels following depletion of *Vps26* alone (**Fig 5E-F**). However, membrane Notch levels were reduced in *Vps35* mutant cells, suggesting that retromer does contribute to Notch trafficking (**Sup Fig 5E**). In addition, *Vps26* depletion had pronounced effects in the context of reduced *Rme-8* (**Fig 5G-H**). The enlarged Notch puncta, characteristic of *Rme-8* depletion, were absent in the combined *Rme-8; Vps26* knockdown (**Fig 5H**). The levels of apical, membrane-associated, Notch were also very strongly reduced in this condition (**Fig 5G**). Moreover, the Rab7 puncta localized more basally, although they were still slightly enlarged compared to WT (**Fig 5H''**). Finally, the TEM suggests that the *Vps26* depletion partially suppressed the MVB enlargement caused by loss of *Rme-8* (**Fig 5I-J, Sup Fig 4G-I**).

In the absence of *Vps26* and *Rme-8*, it appears that Notch is neither recycled to the membrane nor trapped in enlarged endosomes. This fits with the cargo-sorting role of *Vps26* and suggests that, in its absence, Notch fails to become concentrated into a retromer-dependent recycling domain. Instead Notch must be re-directed into other endosomal routes, possibly the endolysosomal pathway where ectopic activation can occur if Notch remains in the limiting membrane (Hori et al., 2011; Wilkin et al., 2008; Wilkin et al., 2004).

### **Removal of ESCRT-0 components in combination with *Rme-8* results in ectopic Notch activation and hyperplastic growth.**

Proteins destined for lysosomal degradation become segregated into ILVs through the activity of four ESCRT complexes (Hurley and Emr, 2006). The first, the ESCRT-0 complex containing Hrs (Hepatocyte growth factor regulated tyrosine kinase substrate) and Stam (Signal transducing adaptor molecule), sorts ubiquitinated cargoes destined for ILVs into clathrin-coated patches. In addition, Hrs has been suggested to act antagonistically towards complexes containing *Rme-8* and retromer to coordinate sorting functions on early endosomes (Popoff et al., 2009). We therefore analyzed the consequences when *Hrs* or *Stam* were depleted in combination with *Rme-8*.

First, we tested effects on *NRE-GFP* expression. As reported (Vaccari et al., 2008), this showed little change following knockdown of either ESCRT-0 (**Fig 6A**). Surprisingly, when either *Hrs* or *Stam* were depleted together with *Rme-8*, *NRE* expression was strongly up-regulated, indicative of extensive ectopic Notch activation (**Fig 6B-C**). This was even greater than that seen with the *Vps26* combination and was

accompanied by concomitant tissue-overgrowth, similar to the hyperplasia observed when other endocytic regulators were compromised (Childress et al., 2006; Moberg et al., 2005; Morrison et al., 2008; Thompson et al., 2005; Vaccari and Bilder, 2005; Vaccari et al., 2008; Vaccari et al., 2009). In general the effects were stronger in the *Stam;Rme-8* combination than in *Hrs;Rme-8* (**Fig 6B-C**), possibly reflecting differences in depletion efficiencies for *Stam* and *Hrs* *Ri* lines, although the latter was nevertheless sufficient to cause substantial reduction in Hrs protein levels (**Sup Fig 5F**).

The outcome on *wg* expression was similar to that on NRE. In *Hrs* or *Stam* single knockdown more Wg accumulated inside receiving cells, suggesting that steady-state levels are affected by the amount of protein routed to lysosomes. However, there was no expansion of the expression-domain (**Fig 6D**). In contrast, when *Rme-8* was depleted together with *Hrs* or *Stam* there was widespread ectopic expression of Wg, similar to NRE (**Fig 6E-F**). Finally, ectopic *NRE-GFP* expression was also seen when *Rme-8 Ri* was expressed in *Hrs* mutant clones (**Sup Fig 5G**). Thus the removal of *Rme-8* uncovers a profound requirement for ESCRT-0 to prevent ectopic Notch activation, which is not evident under normal conditions.

Several studies show that ectopic activation can occur when Notch is trapped at the limiting membrane of mature endosomes marked by Rab7 (Hori et al., 2011; Schneider et al., 2013; Wilkin et al., 2008; Wilkin et al., 2004). As reported previously, in cells depleted for *Hrs* alone Notch accumulated in large Rab7 puncta (**Fig 7A,F**). When *Hrs* and *Rme-8* were knocked-down simultaneously, Notch puncta size increased (**Fig 7B**), and larger Notch-stained structures were detected by super-resolution microscopy (**Fig 7F**). However, the Notch-enriched regions in the combined *Hrs; Rme-8* knockdown were not more coincident with Rab7 (**Fig 7B**) than

in the WT or *Hrs*-depleted tissue (**Fig 4A,E; Fig 7A**) and the super-resolution images from *Hrs;Rme8* tissues did not reveal any increase in overlap between Rab7 and the large Notch conglomerates. Indeed Rab7 was frequently present in dispersed clusters of diffuse small puncta (**Fig 7F**). Finally, the MVBs detected by TEM in this combination were larger than with *Hrs* knockdown alone (**Fig 7C-E**), but the mean perimeter was not significantly different from *Rme-8-Ri* alone (**Sup Fig 4**), suggesting that the MVB is not further enlarged in the double combination. One possibility is that, while the vacuolar endosome/MVB is not enlarged, the Notch tubulated region is more extensive in *Hrs-Ri+Rme-8-Ri* than in *Rme-8-Ri* alone, as suggested by the size of the Notch stained structures in the super resolution images (**Fig 7F, arrows**).

One difference between the Notch accumulations detected in *Hrs* alone compared to the combined knockdown was their apical-basal position as detected in uptake assays. In *Hrs* knockdown, internalized Notch remained trapped close to the apical surface, even after 2 hr (**Fig 7G**). In contrast, when both *Hrs* and *Rme-8* were perturbed, large Notch accumulations were present in basal regions (**Fig 7H**). This result suggests that, when both *Hrs* and *Rme-8* are reduced, Notch becomes trapped at a later stage in the endosomal pathway. In addition, more Notch accumulated than in either single knockdown, consistent with multiple different trafficking routes being perturbed by this combination.

### **Ectopic Notch activation in the *Rme-8* combinations is not dependent on Kuzbanian**

In many instances where Notch becomes activated in the endocytic network, it does not require ligands (Childress et al., 2006; Hori et al., 2004; Jaekel and Klein, 2006; Thompson et al., 2005; Vaccari et al., 2008). To assess whether this might be the case in

the combinations with *Rme-8*, we tested whether activation could be prevented by expression of dominant negative ADAM 10/*Kuzbanian(kuz)*, the protease mediating the ligand-dependent S2 cleavage of Notch. Expression of *kuz<sup>DN</sup>* in either *Vps26;Rme-8* or *ESCRT-0;Rme-8* double knockdown was not able to suppress ectopic *NRE* expression (nor ectopic expression of another Notch target, *deadpan*) although it blocked the normal D/V expression of *NRE* (**Fig 7A-D**). Moreover, expression of *Kuz<sup>DN</sup>* alone prevented D/V boundary expression of *wg*, where it is dependent on Notch activity, without affecting hinge expression hinge, where it is Notch-independent (**Fig 7E**). The former confirmed that *kuz<sup>DN</sup>* was effectively inhibiting ligand dependent signalling, suggesting that the residual *NRE* expression when *kuz<sup>DN</sup>* is combined with *Vps26;Rme-8* or *ESCRT-0;Rme-8* arises through ligand-independent activation. However, expression of *kuz<sup>DN</sup>* did rescue the overgrowth produced by depletion of *ESCRT-0* and *Rme-8* (**Fig 7F-H**). One possible explanation is the positive feedback loop that occurs in this tissue, whereby expression of ligands is positively up-regulated in response to Notch activation (de Celis and Bray, 1997). Hence, any ligand-independent activity might be amplified by subsequent induction of ligand expression. Inhibiting *kuz* function would prevent this amplification, limiting the ectopic Notch activity and tissue overgrowth to that from the ligand-independent route. Alternatively, *kuz* might affect another growth regulatory pathway independent of Notch. Despite these secondary effects, it is evident that a significant proportion of ectopic Notch activation remained in the presence of *kuz<sup>DN</sup>*, suggesting it arose via a ligand-independent mechanism.

## DISCUSSION

Cells continuously internalize Notch, where much of it is routed to lysosomes for degradation. This process must be carefully regulated, not only to ensure steady-state levels of surface expression, but also to prevent inappropriate activation within the endosomal pathway (Childress et al., 2006; Moberg et al., 2005; Morrison et al., 2008; Thompson et al., 2005; Vaccari and Bilder, 2005; Vaccari et al., 2008; Vaccari et al., 2009). Our analysis of *Rme-8* function reveals the importance of another aspect of trafficking, endocytic recycling, in maintaining sufficient levels of Notch at the membrane for signalling to occur correctly. As previous studies have not detected any requirement for retromer in normal Notch pathway function (Belenkaya et al., 2008; Franch-Marro et al., 2008; Pocha et al., 2011), we were surprised to find that Notch pathway activity was sensitive to depletion of *Rme-8*. In addition, the consequences from combined knockdown of *Rme-8* with *Hrs*, *Stam* or *Vps26* show that *Rme-8* is important to prevent inappropriate Notch activation when these cargo-sorting complexes are disrupted. Combined knockdowns resulted in high levels of ectopic Notch signalling and tissue hyperplasia, which could be of significance in the context of recently identified disease-linked mutations in *Rme-8* and other retromer members (McGough et al., 2014; Miura et al., 2014; Vilarino-Guell et al., 2014; Vilariño-Güell et al., 2011; Zavodszky et al., 2014; Zimprich et al., 2011).

In *Rme-8* deficient tissues, Notch accumulated with Rab4 in enlarged endosomal structures and was depleted from the cell surface. Structured illumination microscopy suggested that it was trapped in Rab4-positive tubular structures, which have not previously been detected in *Drosophila*, although tubular Rab5 plasma membrane invaginations have been observed (Fabrowski et al., 2013). FRAP measurements were

compatible with the hypothesis that Notch recycling was compromised under these conditions, making it likely that Rme-8 is necessary for Rab4-mediated recycling and that recycling is important to maintain membrane Notch levels. Notably however, signalling was only detectably impeded when apical levels of Notch were significantly compromised. This is surprising given that Notch activity is dosage sensitive. One possible explanation is that signalling depends critically on the relative levels of Notch and Dl (de Celis and Bray, 1997; Sprinzak et al., 2010) and that, since trafficking of both proteins was perturbed in the *Rme-8* knockdown, the impact may have been lessened. Another possibility is that the Notch pool engaged in functional signalling is localized away from the apical surface, where it is protected from defects in apical recycling. For example some studies have suggested that signalling occurs between basal filopodia (Cohen et al., 2010; De Jossineau et al., 2003) and others have indicated that different receptor pools exist depending on modification state and/or presence of adaptors (Wilkin et al., 2008).

Notch accumulation in *Rme-8* depleted tissue appeared strictly dependant on Vps26, a key component of sorting retromer, while reducing the latter alone had only minor effects on membrane Notch levels. This raises the possibility that another recycling pathway requiring Rme-8 can partially compensate, via the activity of other sorting complexes. One candidate for such alternative sorting could be Hrs, which appears to be involved in sorting cargoes for a fast recycling route as part of the CART complex (actinin-4, BERP, myosinV; Hanyaloglu et al., 2005; Millman et al., 2008; Yan et al., 2004). Conversely, the Snx3-retromer dependant pathway, which recycles Wntless to the Golgi (Harterink et al., 2011; Zhang et al., 2011), appears less sensitive to reductions in Rme-8 than in Vps26, as Wg secretion still occurred in *Rme-8* depleted tissue. This fits with the model that there is spatial separation of SNX3 and SNX-BAR

retromer complexes, which may consequently involve different mechanisms (Burd and Cullen, 2014; Harterink et al., 2011; Mari et al., 2008). Recent data have shown that Rme-8 associates with the WASH complex (Freeman et al., 2014), which is involved in the formation/scission of endosomal tubules as well as in cargo recruitment (Burd and Cullen, 2014; Seaman et al., 2013). Our high-resolution microscopy further suggests that Rme-8 could be involved in tubulation of the sorting endosome in a developmental context. Hence Rme-8 may be specifically required for endosomal routes involving combined actions of retromer and WASH. The possibility that other recycling routes occur independently from Rme-8 would explain why recycling of some receptors, such as the transferrin receptor, still occurs normally when *Rme-8* is knocked down in HeLa cells (Girard and McPherson, 2008).

The ectopic Notch activity in *Rme-8;Vps26* double knockdown was unexpected, since neither single knockdown resulted in receptor activation. The activity was independent of Kuz/Adam10, implying that it was ligand-independent, as seen for other conditions that result in ectopic Notch activation. Such activation is thought to occur when the receptor remains in the limiting membrane of acidifying endosomes where it can be proteolysed to release NICD (Hori et al., 2011; Schneider et al., 2013; Wilkin et al., 2008; Wilkin et al., 2004). With the combined depletion of *Vps26* and *Rme-8*, all endocytosed Notch may thus have been routed towards the endolysosomal pathway where some could fail to be incorporated into ILVs, either because it lacked the appropriate modifications or because the volume exceeded the cargo sorting capacity. No such ectopic Notch activity was seen in the absence of *Vps26* alone, suggesting either that the volume of miss-routed Notch is higher in the *Rme-8;Vps26* depleted conditions, for example if Notch can also be retrieved by *Vps26*-independent

recycling routes that become non-functional when *Rme-8* is missing, or that sorting into ILVs is more disrupted when both are depleted.

More dramatic levels of Notch activation occurred when either ESCRT-0 components, *Stam* or *Hrs*, were perturbed in *Rme-8* depleted cells. Although ESCRT-0 is implicated in sorting ubiquitinated cargo in preparation for its sequestration into ILVs, no ectopic Notch activation was seen when either or both ESCRT-0 components were missing on their own (Tognon et al., 2014; Vaccari et al., 2008). Furthermore, *Hrs* removal can even suppress ectopic Notch activity caused by some other trafficking defects (Childress et al., 2006; Gallagher and Knoblich, 2006; Jaekel and Klein, 2006; Thompson et al., 2005; Troost et al., 2012; Yamada et al., 2011). How can these observations be reconciled with the high level of Notch activation in the combined knockdown of *Rme-8* with *Hrs* or *Stam*? One possibility is that, as with the recycling pathway, there are additional *Rme-8* dependent mechanisms that sort cargoes into ILVs besides *Hrs/Stam*. One candidate is SARA, a FYVE domain protein that forms a complex with RNF11 and that has been reported to function in cargo sorting with ESCRT-0 (Kostaras et al., 2013). SARA partially co-localized with Notch in the *Rme-8* depleted cells and has been associated with Notch activity in some lineages (Coumailleau et al., 2009; Montagne and González-Gaitán, 2014). Another candidate is CD63, a tetraspanin family-member implicated in ESCRT independent sorting of cargoes into ILVs, as well as exosomes (van Niel et al., 2011). Although the function of CD63 homologues has not been explored in *Drosophila*, several tetraspanins affected Notch pathway trafficking or activity in general screens (Dornier et al., 2012; Le Bras et al., 2012). If failure in these, or alternate complexes, can account for the defects brought about by *Rme-8* depletion, it will be interesting to ascertain whether their

deployment also involves the WASH complex, making a link between different Rme-8 dependent routes.

Post-translational modifications also influence ligand independent Notch activity in the endocytic pathway. In particular, Dx mediated Notch ubiquitinylation promotes ligand-independent activation by favouring Notch retention in the limiting membrane of MVBs (Hori et al., 2004; Hori et al., 2011; Wilkin et al., 2008; Yamada et al., 2011). However, *Rme-8* depletion did not modify the Dx over-expression phenotypes. This makes it likely that a different pool of Notch is affected and further suggests that not all endolysosomal trafficking routes depend on Rme-8. This may explain the differing consequences of *Rme-8* depletion on other receptor recycling.

Recent discoveries highlight the importance of Rme-8 as a regulatory node in endocytic trafficking. Notably, mutations in *Rme-8* are found in some patients with familial Parkinson's disease where defects in endocytic trafficking are associated with Lewy bodies (Vilarino-Guell et al., 2014). Rme-8 is also among a small cohort of intracellular transport proteins up-regulated in mammal-infective trypanosomes, suggesting it has a role in controlling the copy number of surface proteins (Koumandou et al., 2013). Here we have demonstrated its importance in Notch receptor recycling, to maintain adequate levels for signalling, which may also be of relevance for these clinical conditions. Furthermore, when combined with defects in *Vps26* or ESCRT-0, reductions in Rme-8 enable high levels of ectopic Notch activation, causing tissue hyperplasia and highlighting the potential hazards when such combinatorial mutations arise.

## MATERIALS AND METHODS

### *Drosophila* genetics

Further details of the stocks used are provided in Table S1. Knockdown of gene expression was achieved using UAS Ri lines (Dietzl et al., 2007; Ni et al., 2011) as follows: UAS-*Rme-8-Ri* (VDRC 22671, 107706), UAS-*w-Ri* (BL 35573), UAS-*Su(H)-Ri* (BL 28900), UAS-*Dx-Ri* (VDRC 7795, 106086); UAS-*Vps26-Ri* (VDRC 18396, BL 38937), UAS-*Hrs-Ri* (BL 33900, 34086), UAS-*Stam-Ri* (VDRC 22497). Additionally UAS-*Kuz<sup>DN</sup>* (BL 6578), UAS-*dx* (Matsuno et al., 2002) and UAS-*Su(Dx)* (Cornell et al., 1999) were used for protein expression. Expression of UAS constructs was driven by *en-GAL4*, *Tub-GAL80<sup>ts</sup>* and larvae were shifted to 30°C 24 hr after egg laying, except that *Rme-8*; *ESCRT0* and *Rme-8*; *Vps26* double knockdown were shifted to 30°C 72 hr after egg laying to avoid lethality. For adult phenotypes, *sal<sup>EPV</sup>-GAL4* (Cruz et al., 2009) was used and crosses were maintained at 25°C until adult eclosion.

Mitotic clones were generated using the FRT/FLP system (Xu and Rubin, 1993). Clones lacking *Rme-8* were obtained using previous characterized X-ray induced loss of function alleles whose phenotypes were reportedly rescued by expression of *Rme-8* (Chang et al., 2004). Clones were generated by crossing *FRT42D Rme-8C<sup>19</sup>/CyO*, *FRT42D Rme-8A<sup>9</sup>/CyO* or *Vps35<sup>[MH20]</sup> FRT42D/CyO* (Franch-Marro et al., 2008) to *hsp-FLP122, tub-Gal4, UAS-GFP; tub-Gal80, FRT42D GFP/CyO* or to *FRT42D PCNA, Ubi-GFP; hh-flp*. To generate *Hrs* mutant clones *Hrs<sup>D28</sup> FRT40A* (Lloyd et al., 2002) was crossed to *hsp-FLP122, tub-Gal4, UAS-GFP; tub-Gal80, FRT40A GFP/CyO; NRE-mCherry*.

Other lines used includes *Gbe+Su(H)-GFP (NRE-GFP)* and *Gbe+Su(H)-mCherry (NRE-mCherry)* (Housden et al., 2012), *tub-Rab4-RFP (Yousefian et al., 2013)*, UAS-*FYVE-GFP*

(Wucherpennig et al., 2003), UAS-*Lamp1-GFP* (BL 42714), *Notch-GFP* (Couturier et al., 2012)

### **Immunostaining and microscopy**

Wing imaginal discs of third-instar larvae were dissected in PBS and fixed in 4% formaldehyde for 20 mins. Discs were washed in PBS-DT (0.3% sodium deoxycholate, 0.3% Triton X-100 in PBS) and blocked in BBT (PBS-DT+1% BSA) before incubation with primary antibodies overnight at 4°C. The following antibodies were used (for further details see Table S2): Mouse anti-NICD (1:20, Developmental Studies Hybridoma Bank [DSHB]; (Fehon et al., 1990), Mouse anti-NECD (1:20, DSHB; Diederich et al., 1994), Rat anti-NECD (1:500, Fehon et al., 1990), Mouse anti-Wg (1:20, DSHB; van den Heuvel et al., 1989), Guinea-Pig anti-Dl (1:3000, Huppert et al., 1997), Rat anti-Ci (1:20 DSHB; Motzny and Holmgren, 1995), Rabbit anti-GFP (1:1000, invitrogen), Rabbit anti-dsRed (1:200, Clontech), Rabbit anti-Rab7 (1:3000) and Rabbit anti-Rab11 (1:8000; Tanaka and Nakamura, 2008), Guinea-Pig anti-Hrs (1:1000, Lloyd et al., 2002), Rabbit anti-Lva (1:500 Sisson et al., 2000), Rabbit anti-Avl (1:1000, Lu and Bilder, 2005), Rabbit anti-Rab5 (1:500, Abcam), GP anti-Vps26 (1:1000, Wang et al., 2014), Rabbit anti-SARA (1:500, Coumailleau et al., 2009). After several washes in PBS-DT, the discs were incubated with fluorescently labelled secondary antibodies, (Jackson Laboratories; details provided in Table S3), for 1-2 hours at room temperature, followed by washing in PBS-DT and labelling with the nuclear marker Hoechst 33342. The samples were mounted in vectashield (vectorlabs) for imaging with Nikon D-Eclipse C1 (PlanFluor 40x 1.30NA oil, PlanApo VC 60x 1.40NA oil objective lenses) or Leica SP2 (63x 1.40NA oil objective lens) confocal microscopes. Samples for High Resolution Microscopy were stained using Alexa Fluor secondary antibodies, and imaged using an OMX-V3 microscope designed

by J.W. Sedat (UCSF, San Francisco, CA) and built by Applied Precision (Gustafsson et al., 2008). This system uses Structured Illumination (SI) where the sample is illuminated with light that has passed through a grating to generate a structured illumination pattern in X, Y and Z. Three cameras oriented in different angles with respect to the sample collect the emitted light (in total, 15 images/focal plane are acquired). The use of post-acquisition algorithms allows reconstruction of the image, giving a resolution below the Abbe limit (~ 120nm in X,Y and 350nm in Z). Post acquisition analysis was performed using Image J, a continuous structure over  $\geq 2$  focal planes that extended from the main circumference of the endosome was considered to be a “tubule”, and the lengths measured accordingly.

### **Notch-uptake Assay**

Imaginal discs were dissected in Schneider's *Drosophila* medium and cultured for 1h at 4°C in the presence of anti-NECD antibody (1:50 DSHB C458.2H, ascites). After three washes with warm media, discs were incubated at 25°C in Schneider's medium with 200 $\mu$ M Chloroquine to block lysosomal degradation (Sigma C-6628; 100mM stock in ddH<sub>2</sub>O). Discs were fixed in 4% formaldehyde at the indicated timepoints, then incubated with anti-Ci and with the appropriate secondary antibodies to reveal protein localization.

### **Transmission Electron Microscopy**

Wing discs were fixed in 2.5% glutaraldehyde in 100 mM phosphate buffer washed in 100 mM phosphate buffer and postfixed in 2% osmium tetroxide in phosphate buffer for 1 hour on ice. After contrasting en bloc in 2% uranyl acetate, the specimens were dehydrated in EtOH and embedded in araldite using acetone as an intermediate

solvent. Thin sections were stained with 2% uranyl acetate and lead citrate. Sections were observed under an EM 902 (Zeiss) microscope at 80 KV.

### **Fluorescence Recovery After Photobleaching (FRAP)**

For FRAP experiments, WT or *Rme-8* depleted wing discs expressing Ni-GFP were dissected in culture media (Schneider's *Drosophila* medium supplemented with 2% FBS, 0.5% penicillin-Streptavidin, and 0.1mg/ml of Ecdysone [Sigma 20-hydroxyecdysone H5142]). Unharmed discs were placed in an observation chamber as previously described (Aldaz et al., 2010) and covered with viscous media (culture media + 2.5x w/v methyl-cellulose (Sigma). For dynasore treatment (Sigma D7693), discs were incubated in Schneider's media containing 100 $\mu$ M dynasore for 30min prior imaging. Image acquisition was performed using an Olympus FV1000 confocal microscope with 100x/1.40 NA oil UPlan-SApochromat objective lens. Stacks of 5z sections spaced by 0.4  $\mu$ m at a speed of 8ms/pixel were acquired before and after bleaching, and then at 7s intervals afterwards. In each half disc, five circular regions of 0.35mm radius were photobleached at apical junctions so that there was only one bleach event per cell. Photobleaching was performed with 10 scans at 8ms/pixel, using 100% 488 laser power. For each field, 3 background, 5 control regions and 5 bleached regions were measured over time, and intensities calculated using ImageJ. Mean fluorescent intensities from background were subtracted from the mean control and mean bleached data sets and, to normalize for fluorescence changes during imaging, the bleached regions were then normalized to controls. At least 2 fields of view were analyzed per disc and 10-12 discs per data set. As described previously for experiments analyzing Cadherin (Bulgakova et al., 2013), each data set was fitted to a biexponential of the form  $f(t) = 1 - F_{im} - A^1 \times e^{-t/T_{fast}} - A^2 \times e^{-t/T_{slow}}$  and to a single exponential of the form  $f(t) = 1 - F_{im} - A^1 \times e^{-t/T_{fast}}$ , where  $F_{im}$  is a size of the

immobile pool of the protein,  $T_{fast}$  and  $T_{slow}$  are the half times, and  $A^1$  and  $A^2$  are the amplitudes of the fast and slow components of the recovery. An F-test was used to assess which of the equations better described each data set. For recovery curves in WT or *Rme-8* depleted tissues, the bi-exponential equation gave the better fit and the resulting p-values are indicated.

**Supplementary material** contains 5 figures and their legends and 3 Tables.

Supplementary Figure S1: *Rme-8* RNAi knock down and phenotypes

Supplementary Figure 2: *Rme-8* appears to regulate Notch trafficking independently of Dx and Su(Dx).

Supplementary Figure S3: Notch associates with enlarged endosomes

Supplementary Figure 4: TEM analysis of *Rme-8*, *Hrs* and *Vps26* knockdowns

Supplementary Figure 5: Retromer and ESCRT-0 RNAi validation and phenotypes

Supplementary Table S1: Details of Drosophila strains

Supplementary Table S2: Details of Primary Antibodies

Supplementary Table S3: Details of Secondary Antibodies

## **ACKNOWLEDGEMENTS**

We thank N. Bulgakova for assistance with FRAP experiments, N. Lawrence for help with OMX, T. Vaccari (IFON, Milan, Italy) for guidance with the uptake assay, H. Bellen (Baylor College of Medicine, Houston, US), D. Bilder (University of California, Berkeley, US) J-P Vincent (NIMR, London, UK) and S. Artavanis-Tsakonas (Harvard Medical School, Boston, US) for sharing reagents. We thank TRiP at Harvard Medical School (NIH/NIGMS R01-GM084947) and VDSC (Vienna, Austria) for transgenic RNAi flies used in this study. This work was funded by an MRC programme grant [G0800034] to

SJB. LAS was the recipient of a BBSRC PhD studentship. ES and TK were funded by the DFG [Sachbeihilfe KL 1028/5-1]. The authors declare no competing financial interests.

## REFERENCES

- Aldaz, S., L.M. Escudero, and M. Freeman. 2010. Live imaging of *Drosophila* imaginal disc development. *Proceedings of the National Academy of Sciences*. 107:14217-14222.
- Baron, M. 2012. Endocytic routes to Notch activation. *Seminars in cell & developmental biology*. 23:437-442.
- Belenkaya, T.Y., Y. Wu, X. Tang, B. Zhou, L. Cheng, Y.V. Sharma, D. Yan, E.M. Selva, and X. Lin. 2008. The retromer complex influences Wnt secretion by recycling wntless from endosomes to the trans-Golgi network. *Developmental Cell*. 14:120-131.
- Bray, S.J. 2006. Notch signalling: a simple pathway becomes complex. *Nature Reviews Molecular Cell Biology*. 7:678-689.
- Brou, C. 2009. Intracellular trafficking of Notch receptors and ligands. *Experimental cell research*. 315:1549-1555.
- Bulgakova, N.A., I. Grigoriev, A.S. Yap, A. Akhmanova, and N.H. Brown. 2013. Dynamic microtubules produce an asymmetric E-cadherin-Bazooka complex to maintain segment boundaries. *The Journal of Cell Biology*. 201:887-901.
- Burd, C., and P.J. Cullen. 2014. Retromer: a master conductor of endosome sorting. *Cold Spring Harbor Perspectives in Biology*. 6.
- Chang, H.C., M. Hull, and I. Mellman. 2004. The J-domain protein Rme-8 interacts with Hsc70 to control clathrin-dependent endocytosis in *Drosophila*. *The Journal of Cell Biology*. 164:1055-1064.
- Childress, J.L., M. Acar, C. Tao, and G. Halder. 2006. Lethal giant discs, a novel C2-domain protein, restricts notch activation during endocytosis. *Current Biology*. 16:2228-2233.
- Cohen, M., M. Georgiou, N.L. Stevenson, M. Miodownik, and B. Baum. 2010. Dynamic Filopodia Transmit Intermittent Delta-Notch Signaling to Drive Pattern Refinement during Lateral Inhibition. *Developmental Cell*. 19:78-89.

- Cornell, M., D.A. Evans, R. Mann, M. Fostier, M. Flaszka, M. Monthatong, S. Artavanis-Tsakonas, and M. Baron. 1999. The *Drosophila melanogaster* Suppressor of *deltex* gene, a regulator of the Notch receptor signaling pathway, is an E3 class ubiquitin ligase. *Genetics*. 152:567-576.
- Coumailleau, F., M. Fürthauer, J.A. Knoblich, and M. González-Gaitán. 2009. Directional Delta and Notch trafficking in Sara endosomes during asymmetric cell division. *Nature*. 458:1051-1055.
- Couturier, L., N. Vodovar, and F. Schweisguth. 2012. Endocytosis by Numb breaks Notch symmetry at cytokinesis. *Nature Cell Biology*. 14:131-139.
- Cruz, C., A. Glavic, M. Casado, and J.F. de Celis. 2009. A Gain-of-Function Screen Identifying Genes Required for Growth and Pattern Formation of the *Drosophila melanogaster* Wing. *Genetics*. 183:1005-1026.
- de Celis, J.F., and S. Bray. 1997. Feed-back mechanisms affecting Notch activation at the dorsoventral boundary in the *Drosophila* wing. *Development*. 124:3241-3251.
- De Jossineau, C., J. Soulé, M. Martin, C. Anguille, P. Montcourrier, and D. Alexandre. 2003. Delta-promoted filopodia mediate long-range lateral inhibition in *Drosophila*. *Nature*. 426:555-559.
- Diederich, R.J., K. Matsuno, H. Hing, and S. Artavanis-Tsakonas. 1994. Cytosolic interaction between *deltex* and Notch ankyrin repeats implicates *deltex* in the Notch signaling pathway. *Development*. 120:473-81.
- Dietzl, G., D. Chen, F. Schnorrer, K.C. Su, Y. Barinova, M. Fellner, B. Gasser, K. Kinsey, S. Oettel, S. Scheiblauer, A. Couto, V. Marra, K. Keleman, and B.J. Dickson. 2007. A genome-wide transgenic RNAi library for conditional gene inactivation in *Drosophila*. *Nature*. 448:151-6.
- Dornier, E., F. Coumailleau, J.F. Ottavi, J. Moretti, C. Boucheix, P. Mauduit, F. Schweisguth, and E. Rubinstein. 2012. TspanC8 tetraspanins regulate ADAM10/Kuzbanian trafficking and promote Notch activation in flies and mammals. *The Journal of Cell Biology*. 199:481-496.
- Fabrowski, P., A.S. Necakov, S. Mumbauer, E. Loeser, A. Reversi, S. Streichan, J.A. Briggs, and S. De Renzis. 2013. Tubular endocytosis drives remodelling of the apical surface during epithelial morphogenesis in *Drosophila*. *Nat Commun*. 4:2244.
- Fehon, R.G., P.J. Kooh, I. Rebay, C.L. Regan, T. Xu, M.A.T. Muskavitch, and S. Artavanis-Tsakonas. 1990. Molecular interactions between the protein products of the neurogenic loci Notch and Delta, two EGF-homologous genes in *Drosophila*. *Cell*. 61:523-534.
- Fortini, M.E., and D. Bilder. 2009. Endocytic regulation of Notch signaling. *Curr Opin Genet Dev*. 19:323-8.

- Franch-Marro, X., F. Wendler, S. Guidato, J. Griffith, A. Baena-Lopez, N. Itasaki, M.M. Maurice, and J.-P. Vincent. 2008. Wingless secretion requires endosome-to-Golgi retrieval of Wntless/Evi/Sprinter by the retromer complex. *Nature Cell Biology*. 10:170-177.
- Freeman, C.L., G. Hesketh, and M.N.J. Seaman. 2014. RME-8 coordinates the activity of the WASH complex with the function of the retromer SNX dimer to control endosomal tubulation. *Journal of cell science*. 127:2053-2070.
- Fujibayashi, A., T. Taguchi, R. Misaki, M. Ohtani, N. Dohmae, K. Takio, M. Yamada, J. Gu, M. Yamakami, M. Fukuda, S. Waguri, Y. Uchiyama, T. Yoshimori, and K. Sekiguchi. 2008. Human RME-8 is involved in membrane trafficking through early endosomes. *Cell structure and function*. 33:35-50.
- Gallagher, C.M., and J.A. Knoblich. 2006. The conserved c2 domain protein lethal (2) giant discs regulates protein trafficking in Drosophila. *Developmental Cell*. 11:641-653.
- Girard, M., and P.S. McPherson. 2008. RME-8 regulates trafficking of the epidermal growth factor receptor. *FEBS Letters*. 582:961-966.
- Girard, M., V. Poupon, F. Blondeau, and P.S. McPherson. 2005. The DnaJ-domain protein RME-8 functions in endosomal trafficking. *The Journal of biological chemistry*. 280:40135-40143.
- Grant, B.D., and J.G. Donaldson. 2009. Pathways and mechanisms of endocytic recycling. *Nature Reviews Molecular Cell Biology*. 10:597-608.
- Gustafsson, M.G., L. Shao, P.M. Carlton, C.J. Wang, I.N. Golubovskaya, W.Z. Cande, D.A. Agard, and J.W. Sedat. 2008. Three-dimensional resolution doubling in wide-field fluorescence microscopy by structured illumination. *Biophys J*. 94:4957-70.
- Hanyaloglu, A.C., E. McCullagh, and M. von Zastrow. 2005. Essential role of Hrs in a recycling mechanism mediating functional resensitization of cell signaling. *The EMBO Journal*. 24:2265-2283.
- Harterink, M., F. Port, M.J. Lorenowicz, I.J. McGough, M. Silhankova, M.C. Betist, J.R.T. van Weering, R.G.H.P. van Heesbeen, T.C. Middelkoop, K. Basler, P.J. Cullen, and H.C. Korswagen. 2011. A SNX3-dependent retromer pathway mediates retrograde transport of the Wnt sorting receptor Wntless and is required for Wnt secretion. *Nature Cell Biology*. 13:914-923.
- Henne, W.M., N.J. Buchkovich, and S.D. Emr. 2011. The ESCRT Pathway. *Developmental Cell*. 21:77-91.

- Hori, K., M. Fostier, M. Ito, T.J. Fuwa, M.J. Go, H. Okano, M. Baron, and K. Matsuno. 2004. Drosophila deltex mediates suppressor of hairless-independent and late-endosomal activation of Notch signaling. *Development*. 131:5527-5537.
- Hori, K., A. Sen, T. Kirchhausen, and S. Artavanis-Tsakonas. 2011. Synergy between the ESCRT-III complex and Deltex defines a ligand-independent Notch signal. *The Journal of Cell Biology*. 195:1005-1015.
- Housden, B.E., K. Millen, S.J. Bray, and B.J. Andrews. 2012. Drosophila Reporter Vectors Compatible with C31 Integrase Transgenesis Techniques and Their Use to Generate New Notch Reporter Fly Lines. *G3&#58; Genes/Genomes/Genetics*. 2:79-82.
- Huppert, S.S., T.L. Jacobsen, and M.A. Muskavitch. 1997. Feedback regulation is central to Delta-Notch signalling required for Drosophila wing vein morphogenesis. *Development*. 124:3283-3291.
- Hurley, J.H., and S.D. Emr. 2006. The ESCRT complexes: structure and mechanism of a membrane-trafficking network. *Annual review of biophysics and biomolecular structure*. 35:277-298.
- Jaekel, R., and T. Klein. 2006. The Drosophila Notch inhibitor and tumor suppressor gene lethal (2) giant discs encodes a conserved regulator of endosomal trafficking. *Dev Cell*. 11:655-69.
- Jovic, M., M. Sharma, J. Rahajeng, and S. Caplan. 2010. The early endosome: a busy sorting station for proteins at the crossroads. *Histology and histopathology*. 25:99-112.
- Kostaras, E., G. Sflomos, N.M. Pedersen, H. Stenmark, T. Fotsis, and C. Murphy. 2013. SARA and RNF11 interact with each other and ESCRT-0 core proteins and regulate degradative EGFR trafficking. *Oncogene*. 32:5220-5232.
- Koumandou, V.L., C. Boehm, K.A. Horder, and M.C. Field. 2013. Evidence for Recycling of Invariant Surface Transmembrane Domain Proteins in African Trypanosomes. *Eukaryotic Cell*. 12:330-342.
- Le Borgne, R., and F. Schweisguth. 2003. Unequal Segregation of Neuralized Biases Notch Activation during Asymmetric Cell Division. *Developmental Cell*. 5:139-148.
- Le Bras, S., C. Rondanino, G. Kriegel-Taki, A. Dussert, and R. Le Borgne. 2012. Genetic identification of intracellular trafficking regulators involved in Notch-dependent binary cell fate acquisition following asymmetric cell division. *Journal of cell science*. 125:4886-4901.
- Li, H., H.-F. Li, R.A. Felder, A. Periasamy, and P.A. Jose. 2008. Rab4 and Rab11 coordinately regulate the recycling of angiotensin II type I receptor as demonstrated by fluorescence resonance energy transfer microscopy. *Journal of Biomedical Optics*. 13:031206.

- Lloyd, T.E., R. Atkinson, M.N. Wu, Y. Zhou, G. Pennetta, and H.J. Bellen. 2002. Hrs regulates endosome membrane invagination and tyrosine kinase receptor signaling in *Drosophila*. *Cell*. 108:261-269.
- Lobry, C., P. Oh, and I. Aifantis. 2011. Oncogenic and tumor suppressor functions of Notch in cancer: it's NOTCH what you think. *Journal of Experimental Medicine*. 208:1931-1935.
- Lu, H., and D. Bilder. 2005. Endocytic control of epithelial polarity and proliferation in *Drosophila*. *Nature Cell Biology*. 7:1232-1239.
- Mari, M., M.V. Bujny, D. Zeuschner, W.J.C. Geerts, J. Griffith, C.M. Petersen, P.J. Cullen, J. Klumperman, and H.J. Geuze. 2008. SNX1 defines an early endosomal recycling exit for sortilin and mannose 6-phosphate receptors. *Traffic*. 9:380-393.
- Matsuno, K., M. Ito, K. Hori, F. Miyashita, S. Suzuki, N. Kishi, S. Artavanis-Tsakonas, and H. Okano. 2002. Involvement of a proline-rich motif and RING-H2 finger of Deltex in the regulation of Notch signaling. *Development*. 129:1049-1059.
- McGough, I.J., and P.J. Cullen. 2011. Recent Advances in Retromer Biology. *Traffic*. 12:963-971.
- McGough, I.J., F. Steinberg, D. Jia, P.A. Barbuti, K.J. McMillan, K.J. Heesom, A.L. Whone, M.A. Caldwell, D.D. Billadeau, M.K. Rosen, and P.J. Cullen. 2014. Retromer binding to FAM21 and the WASH complex is perturbed by the Parkinson disease-linked VPS35(D620N) mutation. *Current biology : CB*. 24:1670-1676.
- Millman, E.E., H. Zhang, H. Zhang, V. Godines, A.J. Bean, B.J. Knoll, and R.H. Moore. 2008. Rapid Recycling of beta(2)-Adrenergic Receptors is Dependent on the Actin Cytoskeleton and Myosin Vb. *Traffic*. 9:1958-1971.
- Miura, E., T. Hasegawa, M. Konno, M. Suzuki, N. Sugeno, N. Fujikake, S. Geisler, M. Tabuchi, R. Oshima, A. Kikuchi, T. Baba, K. Wada, Y. Nagai, A. Takeda, and M. Aoki. 2014. VPS35 dysfunction impairs lysosomal degradation of  $\alpha$ -synuclein and exacerbates neurotoxicity in a *Drosophila* model of Parkinson's disease. *Neurobiology of disease*. 71C:1-13.
- Moberg, K.H., S. Schelble, S.K. Burdick, and I.K. Hariharan. 2005. Mutations in erupted, the *Drosophila* Ortholog of Mammalian Tumor Susceptibility Gene 101, Elicit Non-Cell-Autonomous Overgrowth. *Developmental Cell*. 9:699-710.
- Montagne, C., and M. González-Gaitán. 2014. Sara endosomes and the asymmetric division of intestinal stem cells. *Development*. 141:2014-2023.

- Morrison, H.A., H. Dionne, T.E. Rusten, A. Brech, W.W. Fisher, B.D. Pfeiffer, S.E. Celniker, H. Stenmark, and D. Bilder. 2008. Regulation of early endosomal entry by the *Drosophila* tumor suppressors Rabenosyn and Vps45. *Molecular biology of the cell*. 19:4167-4176.
- Motzny, C.K., and R. Holmgren. 1995. The *Drosophila cubitus interruptus* protein and its role in the wingless and hedgehog signal transduction pathways. *Mech Dev*. 52:137-50.
- Ni, J.Q., R. Zhou, B. Czech, L.P. Liu, L. Holderbaum, D. Yang-Zhou, H.S. Shim, R. Tao, D. Handler, P. Karpowicz, R. Binari, M. Booker, J. Brennecke, L.A. Perkins, G.J. Hannon, and N. Perrimon. 2011. A genome-scale shRNA resource for transgenic RNAi in *Drosophila*. *Nat Methods*. 8:405-7.
- Nolo, R., L.A. Abbott, and H.J. Bellen. 2000. Senseless, a Zn finger transcription factor, is necessary and sufficient for sensory organ development in *Drosophila*. *Cell*. 102:349-62.
- PAN, C., P. BAUM, M. GU, E. JORGENSEN, S. CLARK, and G. GARRIGA. 2008. *C. elegans* AP-2 and Retromer Control Wnt Signaling by Regulating MIG-14/Wntless. *Developmental Cell*. 14:132-139.
- Piddini, E. 2005. Arrow (LRP6) and Frizzled2 cooperate to degrade Wingless in *Drosophila* imaginal discs. *Development (Cambridge, England)*. 132:5479-5489.
- Pocha, S.M., T. Wassmer, C. Niehage, B. Hoflack, and E. Knust. 2011. Retromer controls epithelial cell polarity by trafficking the apical determinant Crumbs. *Curr Biol*. 21:1111-7.
- Popoff, V., G.A. Mardones, S.-K. Bai, V. Chambon, D. Tenza, P.V. Burgos, A. Shi, P. Benaroch, S. Urbé, C. Lamaze, B.D. Grant, G. Raposo, and L. Johannes. 2009. Analysis of articulation between clathrin and retromer in retrograde sorting on early endosomes. *Traffic*. 10:1868-1880.
- Port, F., M. Kuster, P. Herr, E. Furger, C. Bänziger, G. Hausmann, and K. Basler. 2008. Wingless secretion promotes and requires retromer-dependent cycling of Wntless. *Nature Cell Biology*. 10:178-185.
- Rives, A.F., K.M. Rochlin, M. Wehrli, S.L. Schwartz, and S. DiNardo. 2006. Endocytic trafficking of Wingless and its receptors, Arrow and DFrizzled-2, in the *Drosophila* wing. *Developmental biology*. 293:268-283.
- Schneider, M., T. Troost, F. Grawe, A. Martinez-Arias, and T. Klein. 2013. Activation of Notch in *lgd* mutant cells requires the fusion of late endosomes with the lysosome. *J Cell Sci*. 126:645-56.
- Seaman, M.N.J. 2012. The retromer complex - endosomal protein recycling and beyond. *Journal of cell science*. 125:4693-4702.
- Seaman, M.N.J., A. Gautreau, and D.D. Billadeau. 2013. Retromer-mediated endosomal protein sorting: all WASHed up! *Trends in Cell Biology*:1-7.

- Shi, A., L. Sun, R. Banerjee, M. Tobin, Y. Zhang, and B.D. Grant. 2009. Regulation of endosomal clathrin and retromer-mediated endosome to Golgi retrograde transport by the J-domain protein RME-8. *The EMBO journal*. 28:3290-3302.
- Sisson, J.C., C. Field, R. Ventura, A. Royou, and W. Sullivan. 2000. Lava lamp, a novel peripheral golgi protein, is required for *Drosophila melanogaster* cellularization. *The Journal of Cell Biology*. 151:905-918.
- Sönnichsen, B., S. De Renzis, E. Nielsen, J. Rietdorf, and M. Zerial. 2000. Distinct membrane domains on endosomes in the recycling pathway visualized by multicolor imaging of Rab4, Rab5, and Rab11. *The Journal of Cell Biology*. 149:901-914.
- Sprinzak, D., A. Lakhanpal, L. Lebon, L.A. Santat, M.E. Fontes, G.A. Anderson, J. Garcia-Ojalvo, and M.B. Elowitz. 2010. Cis-interactions between Notch and Delta generate mutually exclusive signalling states. *Nature*. 465:86-90.
- Steinberg, F., M. Gallon, M. Winfield, E.C. Thomas, A.J. Bell, K.J. Heesom, J.M. Tavaré, and P.J. Cullen. 2013. A global analysis of SNX27--retromer assembly and cargo specificity reveals a function in glucose and metal ion transport. *Nature Cell Biology*. 15:461-471.
- Tanaka, T., and A. Nakamura. 2008. The endocytic pathway acts downstream of Oskar in *Drosophila* germ plasm assembly. *Development*. 135:1107-1117.
- Temkin, P., B. Lauffer, S. Jäger, P. Cimermancic, N.J. Krogan, and M. von Zastrow. 2011. SNX27 mediates retromer tubule entry and endosome-to-plasma membrane trafficking of signalling receptors. *Nature Cell Biology*. 13:717-723.
- Thompson, B.J., J. Mathieu, H.-H. Sung, E. Loeser, P. Rørth, and S.M. Cohen. 2005. Tumor Suppressor Properties of the ESCRT-II Complex Component Vps25 in *Drosophila*. *Developmental Cell*. 9:711-720.
- Tognon, E., N. Wollscheid, K. Cortese, C. Tacchetti, and T. Vaccari. 2014. ESCRT-0 Is Not Required for Ectopic Notch Activation and Tumor Suppression in *Drosophila*. *PLoS ONE*. 9:e93987.
- Troost, T., S. Jaeckel, N. Ohlenhard, and T. Klein. 2012. The tumour suppressor Lethal (2) giant discs is required for the function of the ESCRT-III component Shrub/CHMP4. *Journal of cell science*. 125:763-776.
- Vaccari, T., and D. Bilder. 2005. The *Drosophila* tumor suppressor vps25 prevents nonautonomous overproliferation by regulating notch trafficking. *Developmental cell*. 9:687-698.

- Vaccari, T., H. Lu, R. Kanwar, M.E. Fortini, and D. Bilder. 2008. Endosomal entry regulates Notch receptor activation in *Drosophila melanogaster*. *The Journal of Cell Biology*. 180:755-762.
- Vaccari, T., T.E. Rusten, L. Menut, I.P. Nezis, A. Brech, H. Stenmark, and D. Bilder. 2009. Comparative analysis of ESCRT-I, ESCRT-II and ESCRT-III function in *Drosophila* by efficient isolation of ESCRT mutants. *Journal of cell science*. 122:2413-2423.
- van den Heuvel, M., R. Nusse, P. Johnston, and P.A. Lawrence. 1989. Distribution of the wingless gene product in *Drosophila* embryos: a protein involved in cell-cell communication. *Cell*. 59:739-49.
- van Niel, G., S. Charrin, S. Simoes, M. Romao, L. Rochin, P. Saftig, M.S. Marks, E. Rubinstein, and G. Raposo. 2011. The tetraspanin CD63 regulates ESCRT-independent and -dependent endosomal sorting during melanogenesis. *Developmental Cell*. 21:708-721.
- Vilarino-Guell, C., A. Rajput, A.J. Milnerwood, B. Shah, C. Szu-Tu, J. Trinh, I. Yu, M. Encarnacion, L.N. Munsie, L. Tapia, E.K. Gustavsson, P. Chou, I. Tatarnikov, D.M. Evans, F.T. Pishotta, M. Volta, D. Beccano-Kelly, C. Thompson, M.K. Lin, H.E. Sherman, H.J. Han, B.L. Guenther, W.W. Wasserman, V. Bernard, C.J. Ross, S. Appel-Cresswell, A.J. Stoessl, C.A. Robinson, D.W. Dickson, O.A. Ross, Z.K. Wszolek, J.O. Aasly, R.M. Wu, F. Hentati, R.A. Gibson, P.S. McPherson, M. Girard, M. Rajput, A.H. Rajput, and M.J. Farrer. 2014. DNAJC13 mutations in Parkinson disease. *Human Molecular Genetics*. 23:1794-1801.
- Vilariño-Güell, C., C. Wider, O.A. Ross, J.C. Dachselt, J.M. Kachergus, S.J. Lincoln, A.I. Soto-Ortolaza, S.A. Cobb, G.J. Wilhoite, J.A. Bacon, B. Behrouz, H.L. Melrose, E. Hentati, A. Puschmann, D.M. Evans, E. Conibear, W.W. Wasserman, J.O. Aasly, P.R. Burkhard, R. Djaldetti, J. Ghika, F. Hentati, A. Krygowska-Wajs, T. Lynch, E. Melamed, A. Rajput, A.H. Rajput, A. Solida, R.-M. Wu, R.J. Uitti, Z.K. Wszolek, F. Vingerhoets, and M.J. Farrer. 2011. VPS35 mutations in Parkinson disease. *American journal of human genetics*. 89:162-167.
- Wang, S., K.L. Tan, M.A. Agosto, B. Xiong, S. Yamamoto, H. Sandoval, M. Jaiswal, V. Bayat, K. Zhang, W.-L. Charng, G. David, L. Duraine, K. Venkatachalam, T.G. Wensel, and H.J. Bellen. 2014. The Retromer Complex Is Required for Rhodopsin Recycling and Its Loss Leads to Photoreceptor Degeneration. *PLoS Biology*. 12:e1001847.
- Wilkin, M., P. Tongngok, N. Gensch, S. Clemence, M. Motoki, K. Yamada, K. Hori, M. Taniguchi-Kanai, E. Franklin, K. Matsuno, and M. Baron. 2008. *Drosophila* HOPS and AP-3 Complex Genes Are Required for a Deltex-Regulated Activation of Notch in the Endosomal Trafficking Pathway. *Developmental Cell*. 15:762-772.

- Wilkin, M.B., A.-M. Carbery, M. Fostier, H. Aslam, S.L. Mazaleyrat, J. Higgs, A. Myat, D.A.P. Evans, M. Cornell, and M. Baron. 2004. Regulation of Notch Endosomal Sorting and Signaling by *Drosophila* Nedd4 Family Proteins. *Current Biology*. 14:2237-2244.
- Wucherpennig, T., M. Wilsch-Bräuninger, and M. González-Gaitán. 2003. Role of *Drosophila* Rab5 during endosomal trafficking at the synapse and evoked neurotransmitter release. *The Journal of Cell Biology*. 161:609-624.
- Xu, T., and G.M. Rubin. 1993. Analysis of genetic mosaics in developing and adult *Drosophila* tissues. *Development*. 117:1223-1237.
- Yamada, K., T.J. Fuwa, T. Ayukawa, T. Tanaka, A. Nakamura, M.B. Wilkin, M. Baron, and K. Matsuno. 2011. Roles of *Drosophila* Deltex in Notch receptor endocytic trafficking and activation. *Genes to Cells*. 16:261-272.
- Yan, Q., W. Sun, P. Kujala, Y. Lotfi, T.A. Vida, and A.J. Bean. 2004. CART: an Hrs/actinin-4/BERP/myosin V protein complex required for efficient receptor recycling. *Molecular Biology of the Cell*. 16:2470-2482.
- YANG, P., M. LORENOWICZ, M. SILHANKOVA, D. COUDREUSE, M. BETIST, and H. KORSWAGEN. 2008. Wnt Signaling Requires Retromer-Dependent Recycling of MIG-14/Wntless in Wnt-Producing Cells. *Developmental Cell*. 14:140-147.
- Yousefian, J., T. Troost, F. Grawe, T. Sasamura, M. Fortini, and T. Klein. 2013. Dmon1 controls recruitment of Rab7 to maturing endosomes in *Drosophila*. *Journal of cell science*. 126:1583-1594.
- Zavodszky, E., M.N. Seaman, K. Moreau, M. Jimenez-Sanchez, S.Y. Breusegem, M.E. Harbour, and D.C. Rubinsztein. 2014. Mutation in VPS35 associated with Parkinson's disease impairs WASH complex association and inhibits autophagy. *Nature communications*. 5.
- Zhang, P., Y. Wu, T.Y. Belenkaya, and X. Lin. 2011. SNX3 controls Wingless/Wnt secretion through regulating retromer-dependent recycling of Wntless. *Cell Research*. 21:1677-1690.
- Zhang, Y., B. Grant, and D. Hirsh. 2001. RME-8, a conserved J-domain protein, is required for endocytosis in *Caenorhabditis elegans*. *Molecular biology of the cell*. 12:2011-2021.
- Zimprich, A., A. Benet-Pagès, W. Struhal, E. Graf, S.H. Eck, M.N. Offman, D. Haubenberger, S. Spielberger, E.C. Schulte, P. Lichtner, S.C. Rossle, N. Klopp, E. Wolf, K. Seppi, W. Pirker, S. Presslauer, B. Mollenhauer, R. Katzenschlager, T. Foki, C. Hotzy, E. Reinthaler, A. Harutyunyan, R. Kralovics, A. Peters, F. Zimprich, T. Brücke, W. Poewe, E. Auff, C. Trenkwalder, B. Rost, G. Ransmayr, J.

Winkelman, T. Meitinger, and T.M. Strom. 2011. A mutation in VPS35, encoding a subunit of the retromer complex, causes late-onset Parkinson disease. *American journal of human genetics*. 89:168-175.

## FIGURE LEGENDS

### Figure 1: Rme8 regulates Notch pathway function.

**(A)** *Sal<sup>PEv</sup>-Gal4* expression domain in an adult wing.

**(B-D)** Adult wing from flies expressing *w* (B), *Rme-8* (C) or *Su(H)* (D) *Ri* with *Sal<sup>PEv</sup>-Gal4*. *Rme-8* knockdown results in vein thickening and small deltas, similar to *Su(H)-Ri* treatment (arrows). Also note loss of posterior cross vein (arrowhead, Pcv). L2-5 veins; Acv, anterior cross-vein.

**(E)** *en-Gal4* expression domain in the posterior wing disc, as used in this and all subsequent knockdown experiments **(F-H)** NRE-mCherry expression in wing discs from flies expressing *w* (F), *Rme-8* (G) or *Su(H)* (H) *Ri* (right of dashed line). *Rme-8-Ri* slightly reduced *NRE* expression, *Su(H)-Ri* causes loss of *NRE* expression. Ci marks the unaffected anterior compartment in this and all subsequent experiments

**(I)** NRE-mCherry expression is decreased in *Rme-8* (*Rme-8<sup>C19</sup>*) mutant cells (GFP-ve). Mutant clones were generated using *FRT42D PCNA, Ubi-GFP;hh-flp*

**(J)** A/P pixel intensity ratio, measured in comparable posterior and anterior regions of control, *Rme<sup>C19</sup>* mutant (*C19*; *n*=7) *Rme-8* knockdown (*Rme-8Ri*, *n*=12) discs.

### Figure 2: Aberrant trafficking of Notch, Dl and Wg in *Rme-8* depleted cells

**(A-B)** Effects of *Rme-8 Ri* on Notch (anti-NICD, red in A-B; anti-NECD, green in B) and Dl (green in A) trafficking. Both, full-length Notch and Dl accumulate together inside *Rme-8-Ri* cells (arrowhead). Depleted territory in this and subsequent figures is on the right side of dashed line.

**(C)** NECD (staining without detergent) is depleted from the membrane when *Rme-8* is knocked-down (*Rme-8<sup>KK</sup>*).

**(D)** Quantification of surface NECD levels from (C). The data shown are from a single representative disc, n= 6 for the experiment shown; the experiment was repeated 3 times with similar results.

**(E)** Intracellular Notch puncta accumulate in *Rme-8<sup>C19</sup>* mutant cells (GFP-ve), (generated as in Fig 1I)

**(F)** Wg (red) is detected more broadly in the *Rme-8-Ri* tissue.

### **Figure 3: Notch accumulates in subapical puncta in Rme-8 depleted cells**

**(A-C)** Antibody uptake assay to detect Notch trafficking (anti-NECD) in cultured wing discs. Different focal planes (apical, A, B, C; sub-apical B', C'; basal B'', C'') from xy sections at 0min (A), 30min (B) or 2h (C) after uptake.

**(D-F)** xz cross-sections of discs in A, B and C, respectively. Notch-antibody complexes accumulate sub-apically in *Rme-8-Ri* (right) after 30min but accumulate more basally in WT (left).

**(G)** Quantification of fluorescence levels from Notch-antibody complexes according to distance from apical membrane in xz cross-sections (apical levels were normalised to 1 for comparisons between samples). At 30min and 2h more anti-NECD is detected in sub-apical regions with *Rme-8-Ri* compared to WT.

**(H)** Comparison between sub-apical levels of anti-NECD detected at different time-points in WT (WT) and *Rme-8 Ri* tissue.

**(I)** Quantification of apical-membrane anti-NECD in anterior (left, WT) versus posterior (right, *Rme-8 Ri*) of discs in A-C. The data shown are from a single representative disc, n= 10 for the experiment shown; the experiment was repeated 2 times with similar results.

**Figure 4: Notch associates with enlarged endosomes and recovers more slowly at the membrane in *Rme-8* depleted cells.**

**(A)** Enlarged puncta containing NICD, Rab4 and Rab7 are detected in *Rme8-Ri*, where NICD accumulates in proximity to Rab4 (see insets).

**(B)** Enlarged puncta containing NICD, Rab4 and Rab11 were detected in *Rme-8-Ri* cells. Some puncta contain all 3 proteins (inset, yellow arrowhead), others contain Rab11 only (inset, green arrowhead) or Rab4+NICD (inset, red arrowhead).

**(C-F)** Super-resolution images of endosomes from WT (C, E) or *Rme-8-Ri* (D, F) wing-disc cells stained for NICD and Rab4 (C-D) or Rab7 (E-F). Notch localizes adjacent to Rab4 in protrusions (arrows, C). In *Rme-8*-depleted cells tubule-like protrusions appear more extensive (arrows, D). Rab7 labels a compartment adjacent to NICD accumulations, both in WT and *Rme-8-Ri* cells (arrowheads, E, F).

**(G)** Measurements of protruding Rab4-labelled tubule-like structures on endosomes from WT and *Rme-8* knockdown ( $\geq 50$  tubules/disc; 5 discs per genotype).

**(H, I)** Sections from WT (H) or *Rme-8-Ri* (I) regions of a wing disc analyzed by TEM, with endosomes highlighted in yellow.

**(J)** Quantification of endosome perimeters from TEM images. (WT n=28, *Rme-8-i+w-Ri* n=76).

**(K-L)** FRAP experiments, measuring recovery of Notch-GFP after photo-bleaching. (K) Plot of averaged recovery curves (mean  $\pm$  SEM) with best-fit curves as solid lines. (L) Single FRAP examples with red circles showing bleach spots. (P=prebleach). The recovery curves could be described by a bi-exponential equation (wt,  $p < 0.0001$ ; *Rme-8*,  $p = 0.02$ ; Bulgakova et al., 2013; see methods) suggestive of two recovery processes, fast diffusion within the membrane and slower endocytic trafficking. Both appear affected by *Rme-8* depletion.

**Figure 5: Combined depletion of *Rme-8* with *Vps-26* results in ectopic Notch activation.**

**(A, B)** NRE-mCherry is ectopically expressed in *Vps26-Ri;Rme8-Ri* (B) compared with *Vps26-Ri;w-Ri* (A)

**(C, D)** Wg accumulates inside both producing and receiving cells in *Vps26-Ri;Rme8-Ri* (D) but only in producing cells in *Vps26-Ri;w-Ri* (C).

**(E-H)** NICD and Rab7 distribution in *Vps26-Ri;w-Ri* (E-F), or *Vps26-Ri;Rme-8-Ri* (G-H) wing discs. Apical (E, G) and sub-apical focal planes (F,H) with xz cross-sections from discs in F and H beneath.

**(I-J)** TEM images of *Vps26-Ri;Rme8-Ri* (I) with endosomes coloured in yellow, and quantification of endosomal perimeter from TEM images (J) (WT n=83, *Vps26-Ri+Rme-8-Ri* n=30).

**Figure 6: Combined depletion of *Rme-8* with *ESCRT-0* results in ectopic Notch activation and tissue over-growth.**

**(A-F)** NRE-GFP (A-C) and Wg (D-F) expression are strongly up-regulated in *Hrs+Rme-8* double knockdown (B, E) and *Stam+Rme8* double knockdown (C, F), in contrast to the *Hrs* single knockdown where expression is unaffected (A, D, *Hrs-Ri;w-Ri*).

**Figure 7: Effects on Notch trafficking of combined *Rme-8* and *ESCRT-0* depletion.**

**(A-B)** Distribution of NICD and Rab7. xy section of discs at the sub-apical plane (upper panel) and xz cross-sections of the same specimens (lower panel). Notch accumulates in enlarged Rab7 structures upon *Hrs* knockdown (A; *Hrs-Ri+w-Ri*) but not in double knockdown (B; *Hrs-Ri+Rme8-Ri*).

**(C-D)** TEM images of *Hrs-Ri;w-Ri* (C) or *Hrs-Ri;Rme8-Ri* (D) with endosomes coloured in yellow.

(E) Quantification of endosome perimeters from TEM images (WT n=83, *Hrs-Ri+w-Ri* n=33, *Hrs-Ri+Rme-8-Ri* n=42).

(F) Super-Resolution images of single endosomes from *Hrs-Ri;w-Ri* (left panel) or *Hrs-Ri;Rme8-Ri* (right panel) expressing discs, stained for NICD and Rab7 that appear to localize in the same vesicular compartment in *Hrs* knockdown (arrowheads, left panel), but not in the *Rme-8-Hrs* double knockdown, where N localizes in long tubules (arrows, right panel).

(G-H) Antibody uptake assay for Notch in cultured wing imaginal discs expressing *Hrs-Ri;w-Ri* (G) or *Hrs-Ri;Rme8-Ri* (H).

**Figure 8: Ectopic Notch activation observed in combined depletions is not prevented by *kuz<sup>DN</sup>***

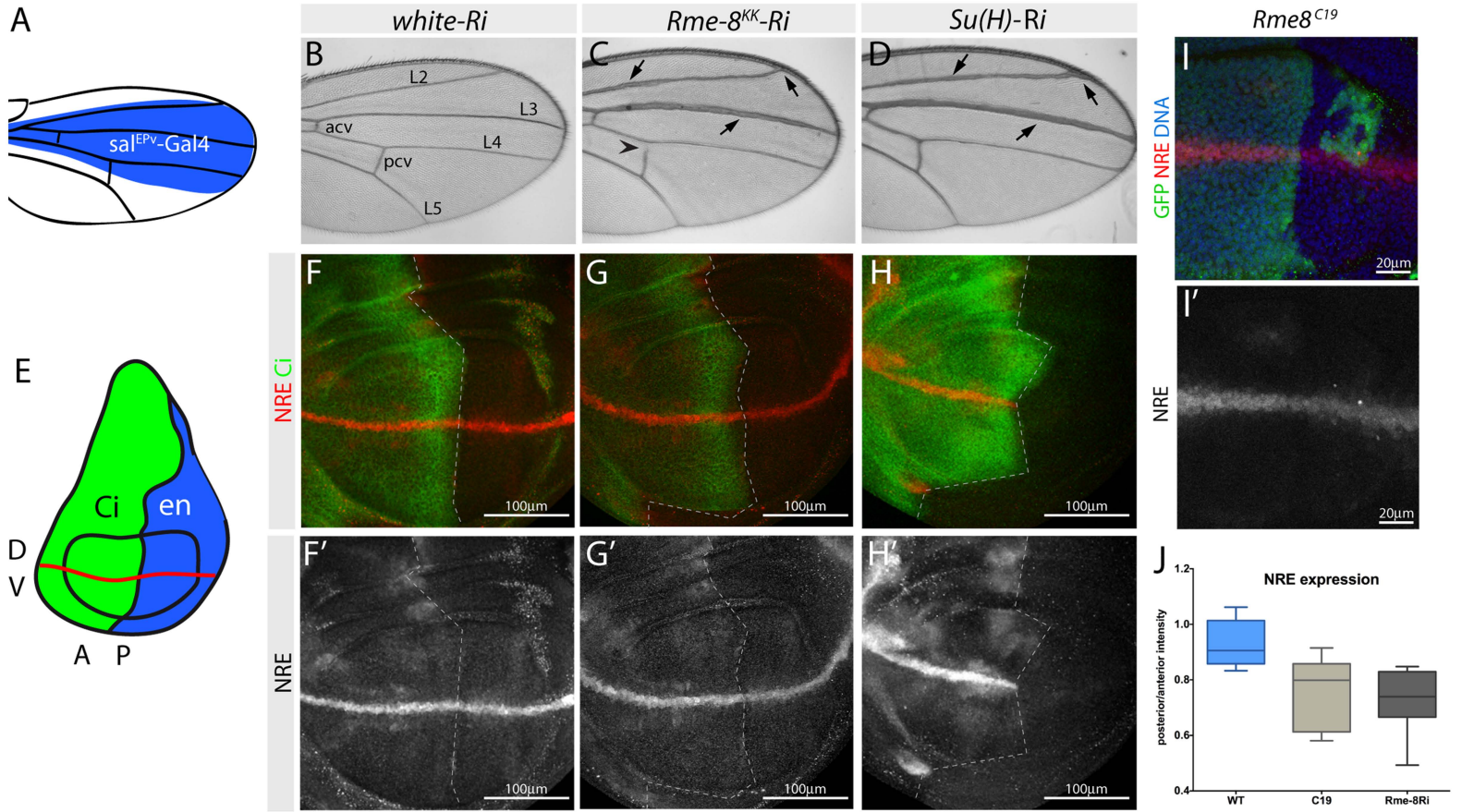
(A-D) NRE-GFP expression shows that ectopic Notch activation in *StamRi+Rme-8-Ri* (A) or *Vps26-Ri+Rme-8-Ri* (C) is not rescued by *kuz<sup>DN</sup>* co-expression (B, D).

(E) Wg D/V expression is lost in discs expressing *kuz<sup>DN</sup>* alone.

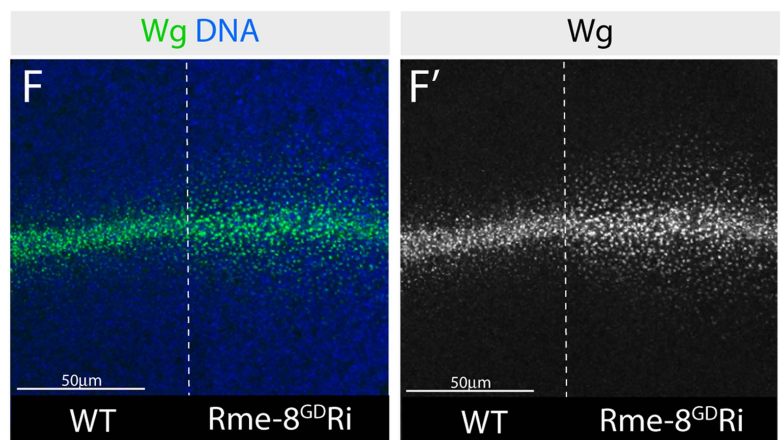
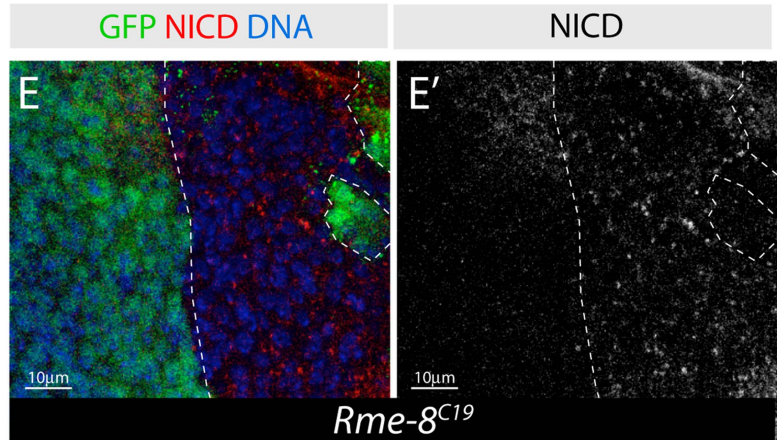
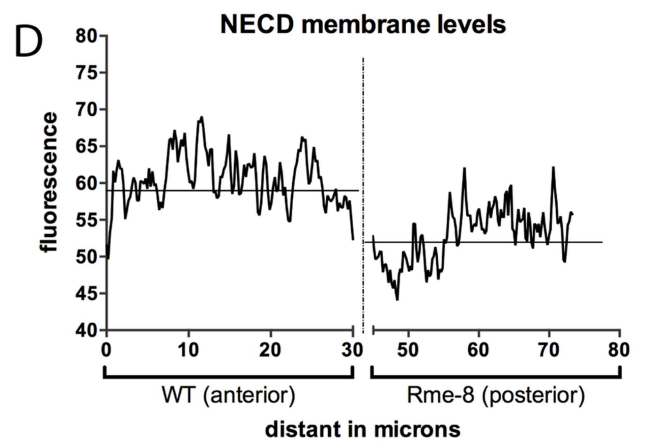
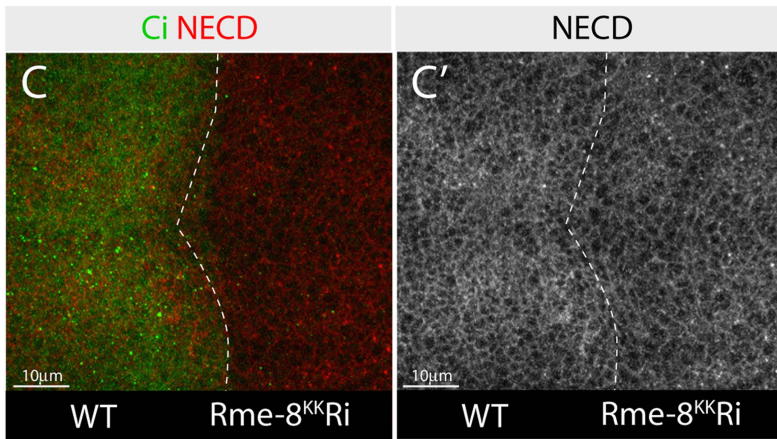
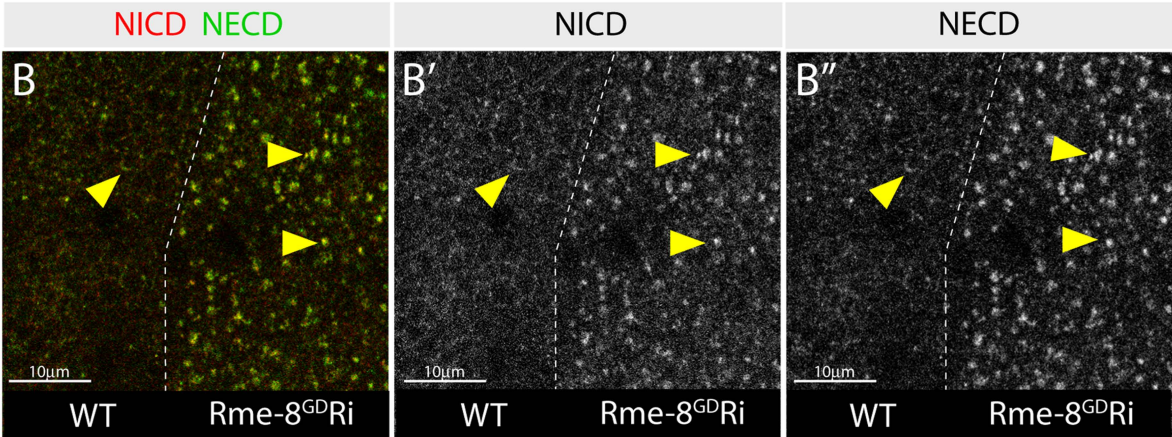
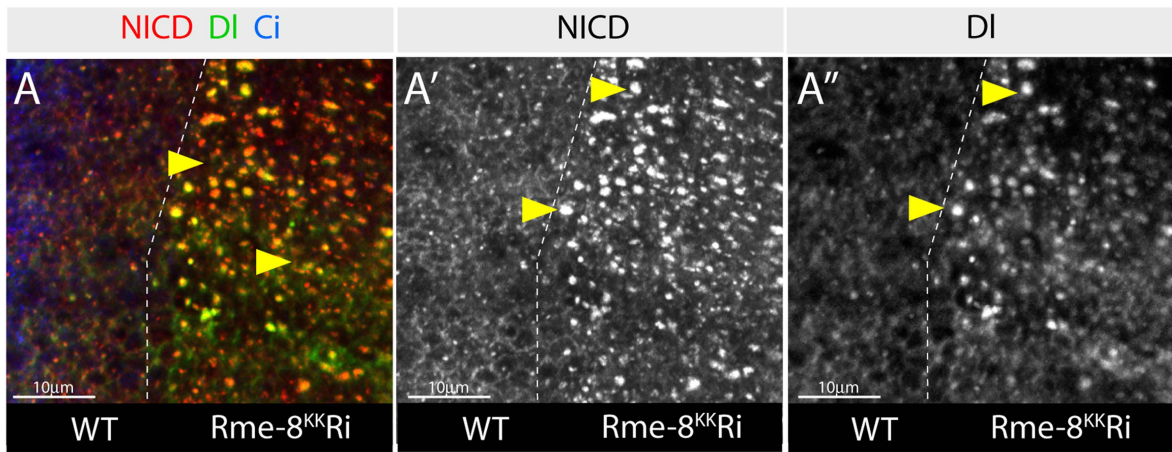
(F-G) *kuz<sup>DN</sup>* co-expression rescues overgrowth caused by *Hrs-Ri+Rme-8-Ri*.

(H) Quantification of wing disc size for genotypes shown in F, G.

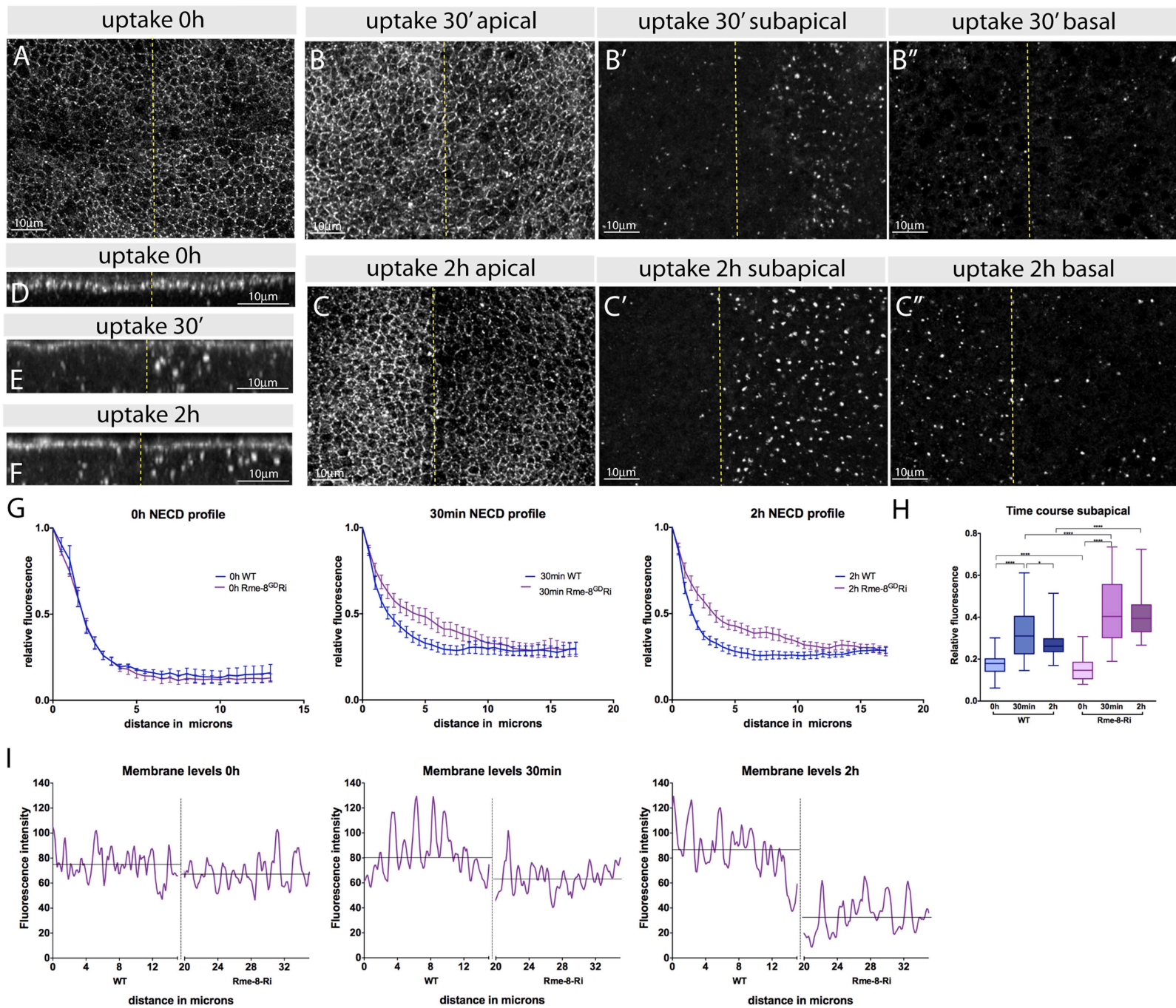
# Gomez-Lamarca, Figure 1



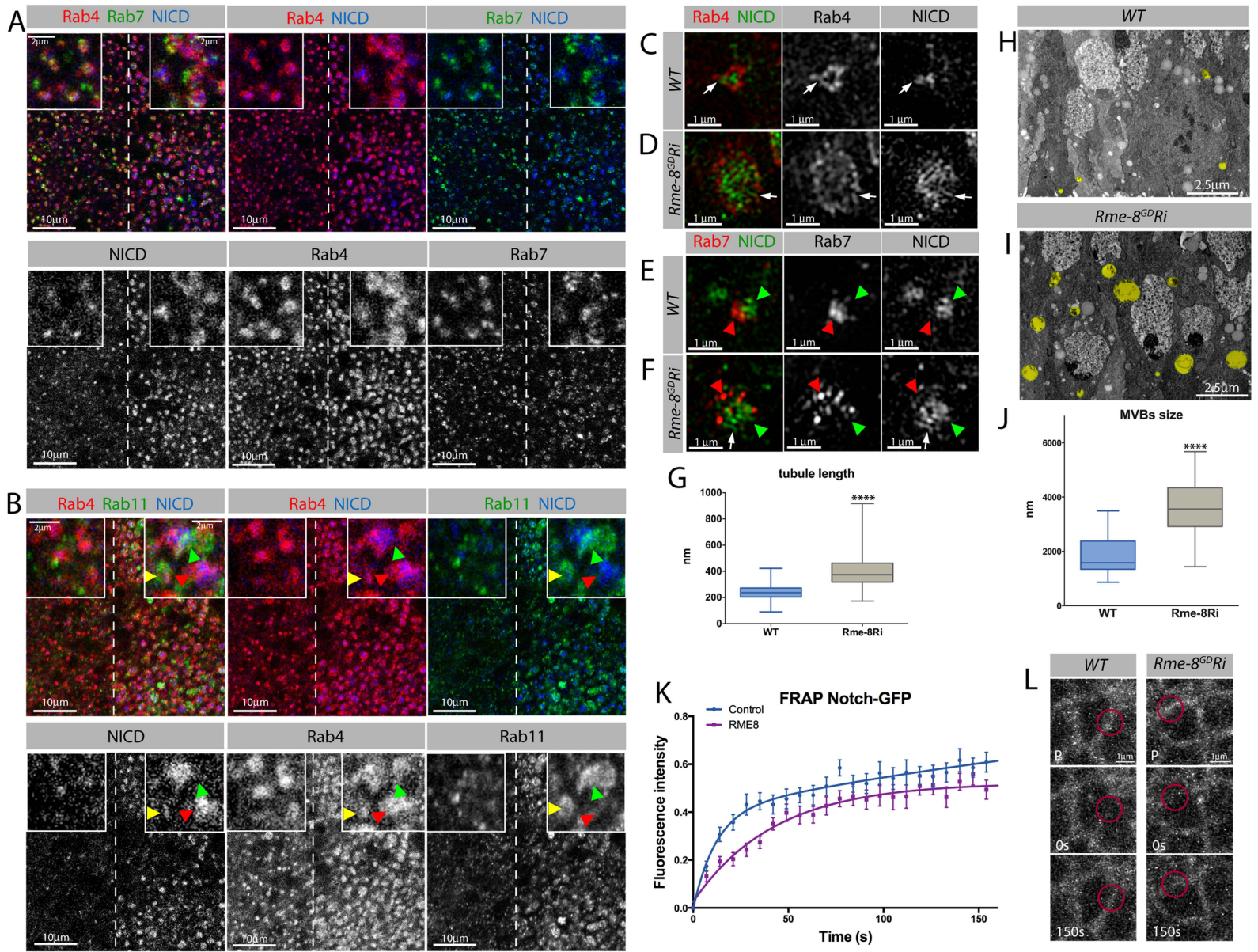
Gomez-Lamarca, Figure 2



# Gomez-Lamarca, Figure 3



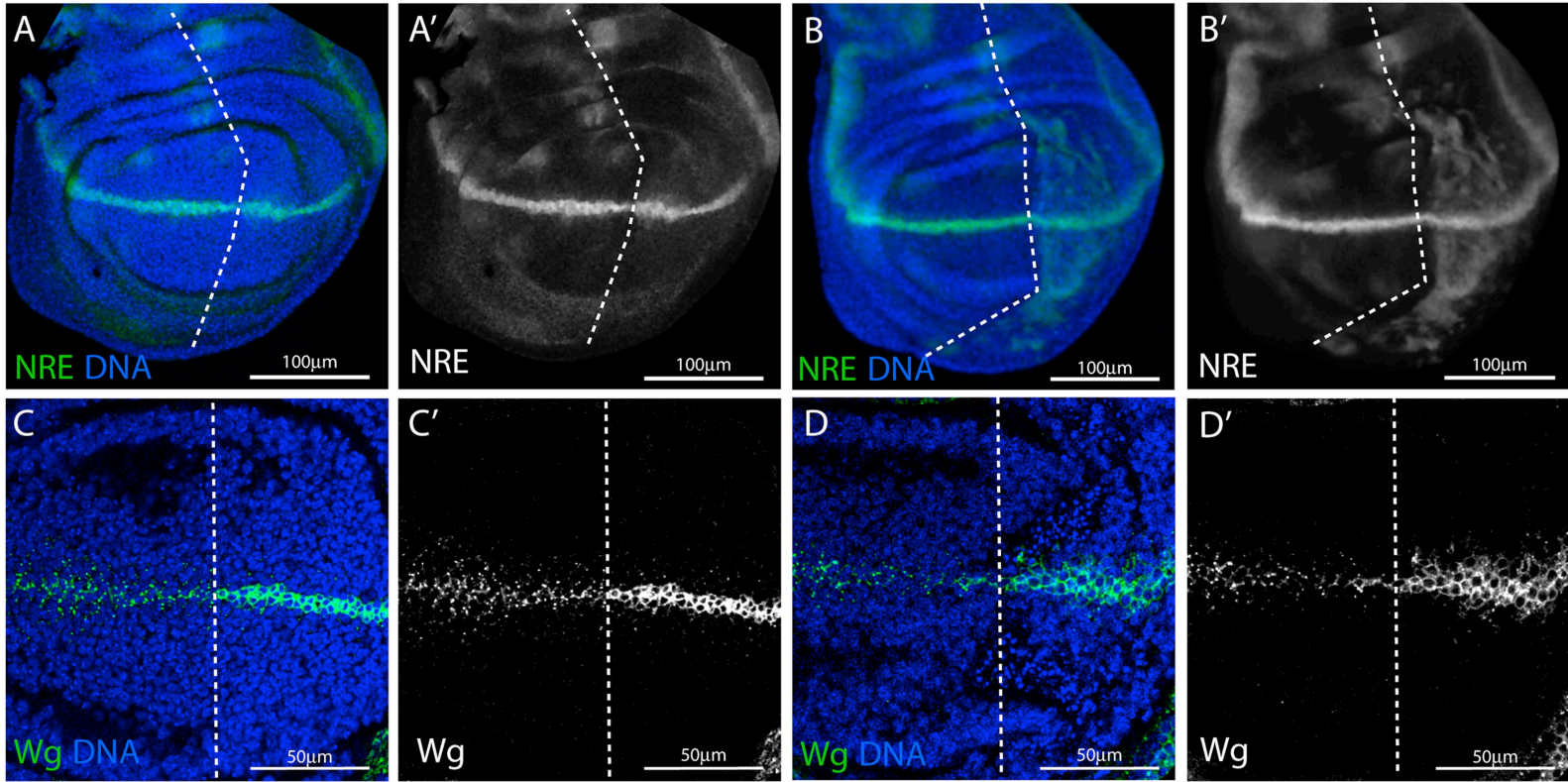
# Gomez-Lamarca, Figure 4



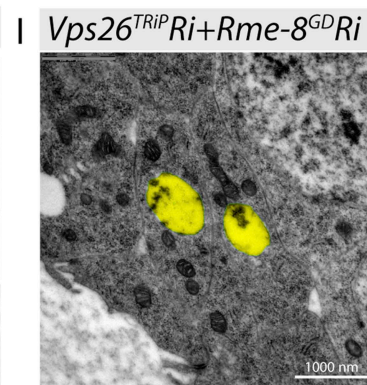
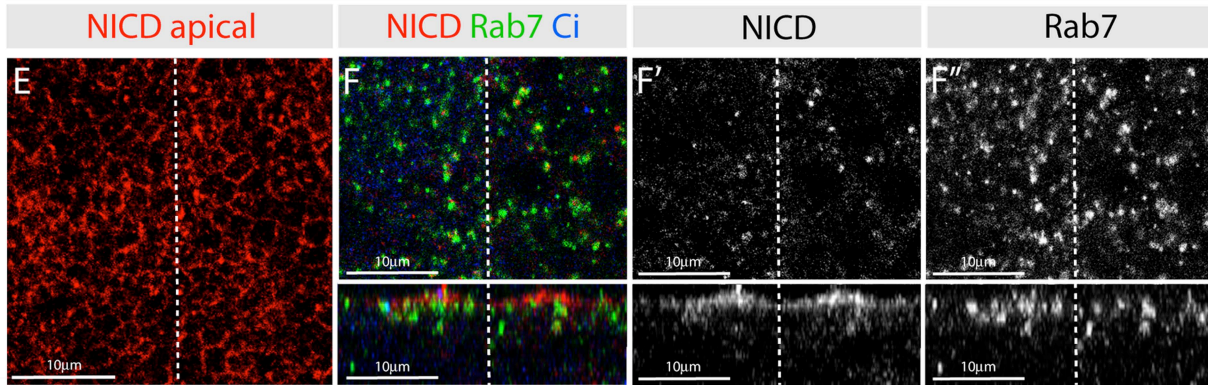
Gomez-Lamarca, Figure 5

*Vps26<sup>TRIP</sup>Ri+white-Ri*

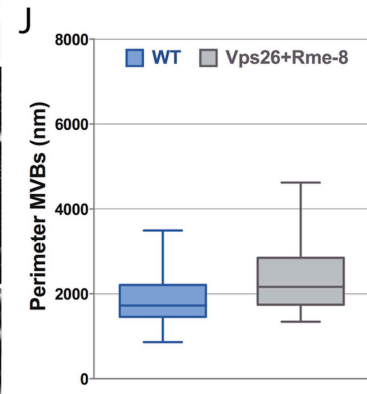
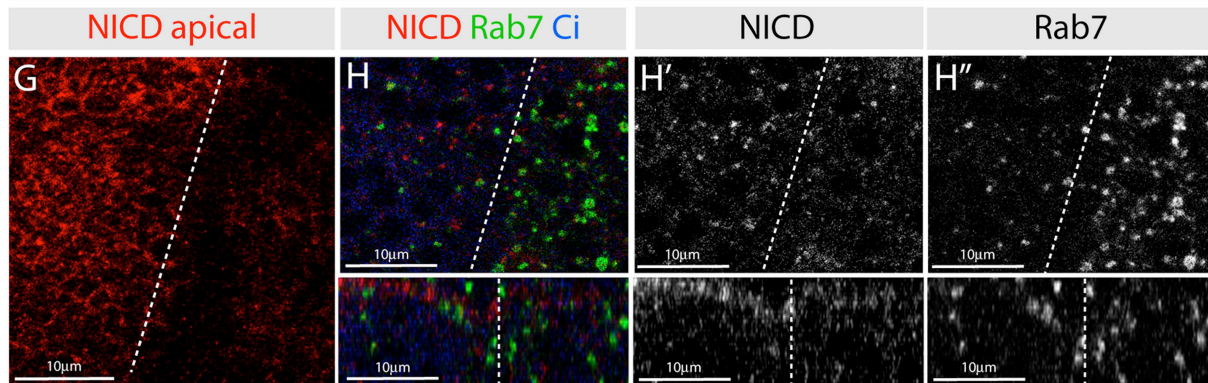
*Vps26<sup>TRIP</sup>Ri+Rme-8<sup>GD</sup>Ri*



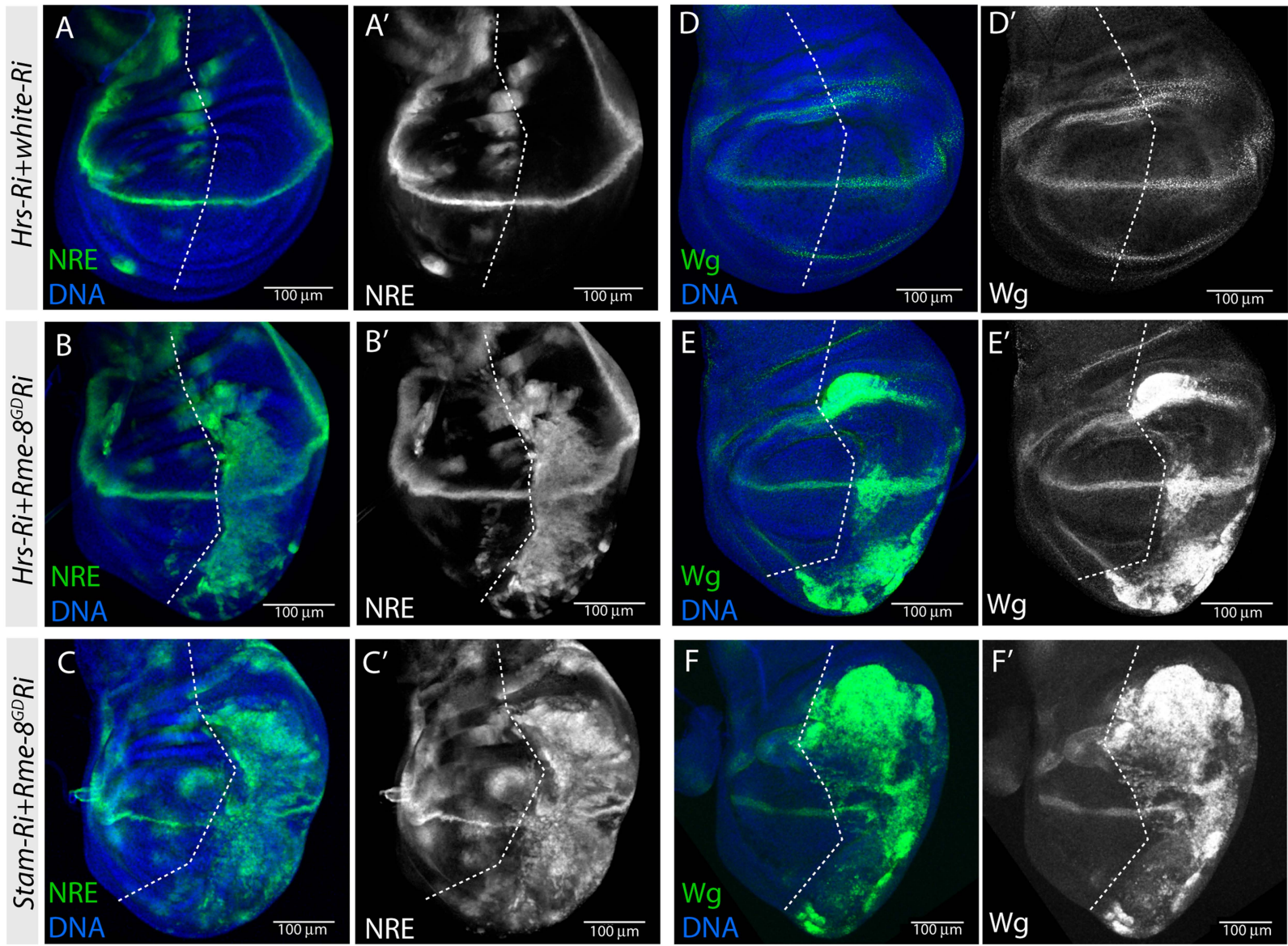
*Vps26<sup>GD</sup>Ri+white-Ri*



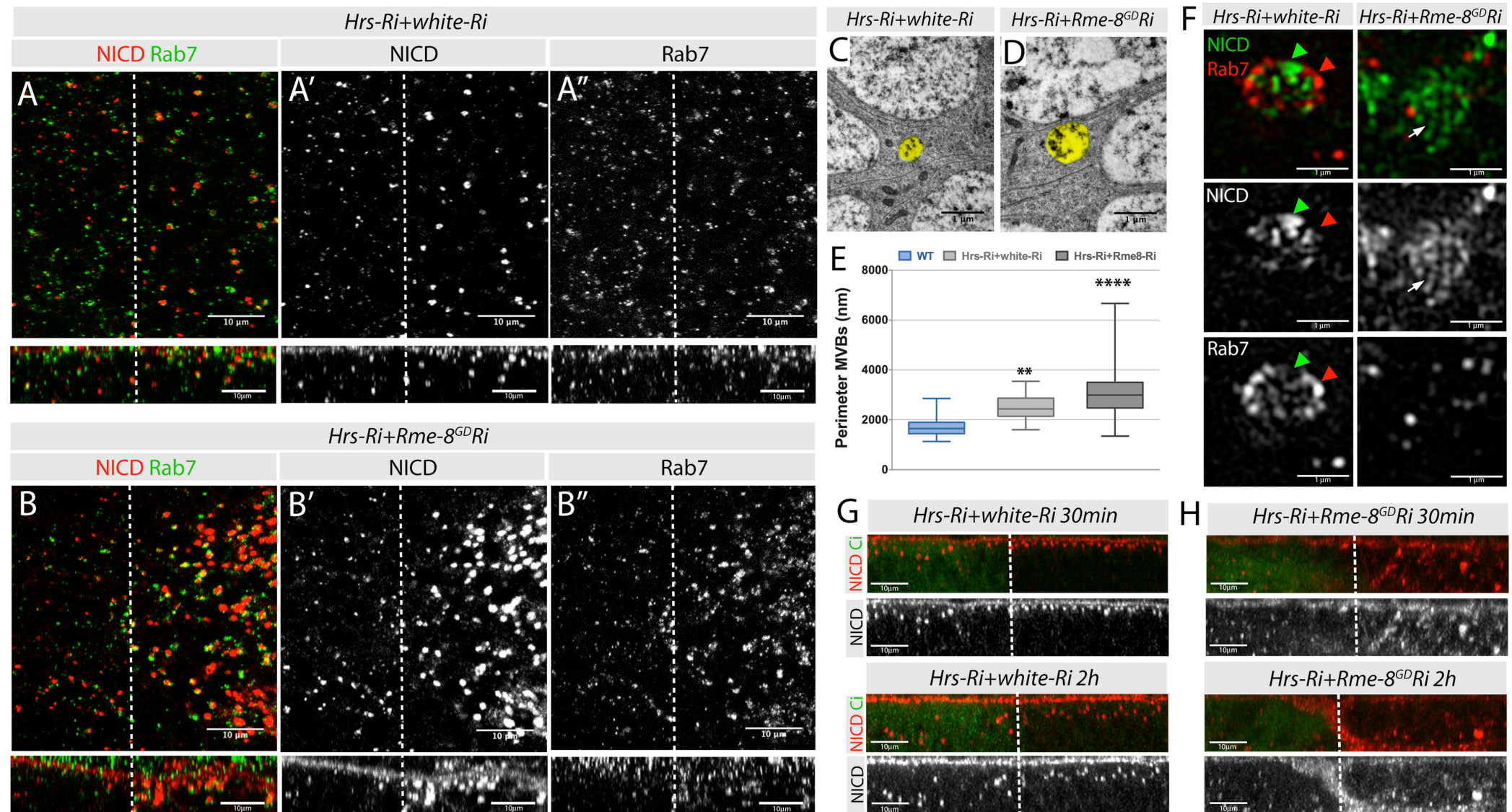
*Vps26<sup>GD</sup>Ri+Rme-8<sup>GD</sup>Ri*



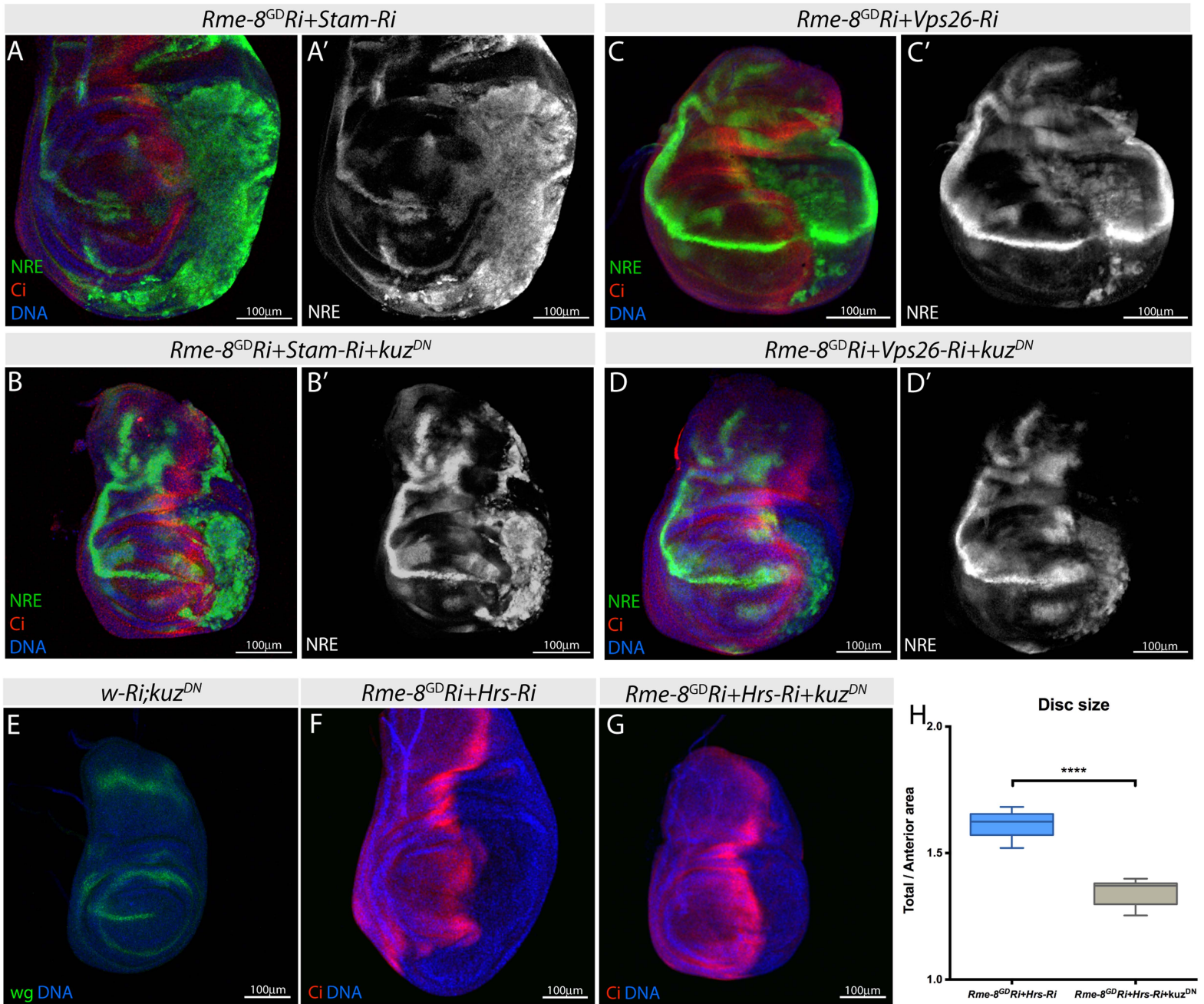
Gomez-Lamarca, Figure 6



Gomez-Lamarca, Figure 7



Gomez-Lamarca, Figure 8



## **SUPPLEMENTARY MATERIAL**

Supplementary Figure S1: *Rme-8 RNAi* knock down and phenotypes

Supplementary Figure S2: *Rme-8* appears to regulate Notch trafficking independently of Dx and Su(Dx).

Supplementary Figure S3: Notch associates with enlarged endosomes

Supplementary Figure S4: TEM analysis of *Rme-8*, *Hrs* and *Vps26* knockdowns

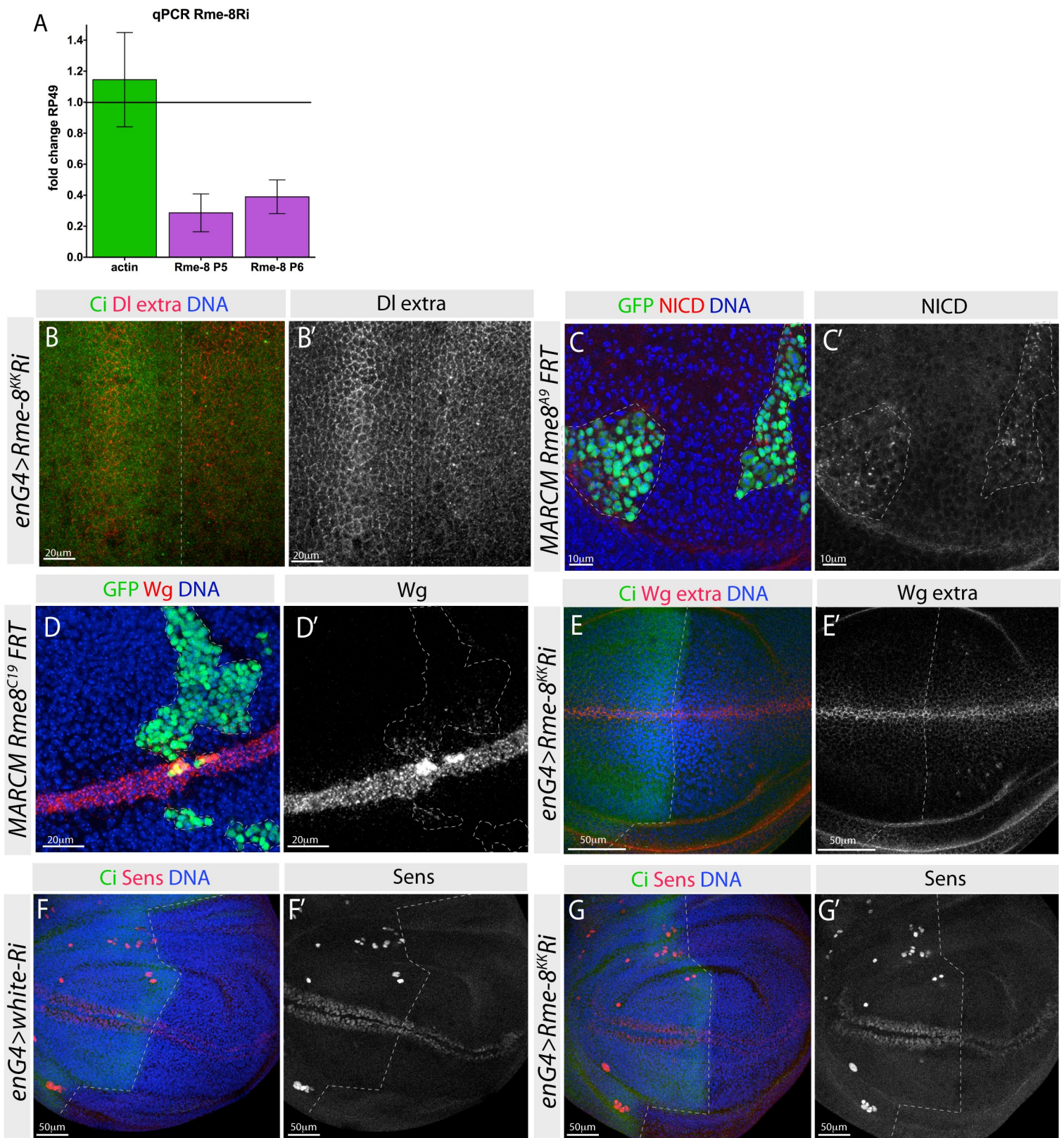
Supplementary Figure S5: Retromer and ESCRT-0 RNAi validation and phenotypes

Supplementary Table S1: Details of *Drosophila* strains

Supplementary Table S2: Details of Primary Antibodies

Supplementary Table S3: Details of Secondary Antibodies

# Gomez-Lamarca, Supplementary Figure 1



## Supplementary Figure 1: Rme-8 RNAi knock down and phenotypes

**(A)** Graph showing reduction of *Rme-8* mRNA levels respect to those of a highly expressed gene, *actin*, measured by qPCR using two pairs of primers that target different regions of the gene.

**(B)** Wing imaginal disc stained for Ci (green), Dl extracellular (red in B; white in B') and Hoescht (blue), shows reduction of Dl membrane levels in *Rme-8* knock-down cells (right from dotted line).

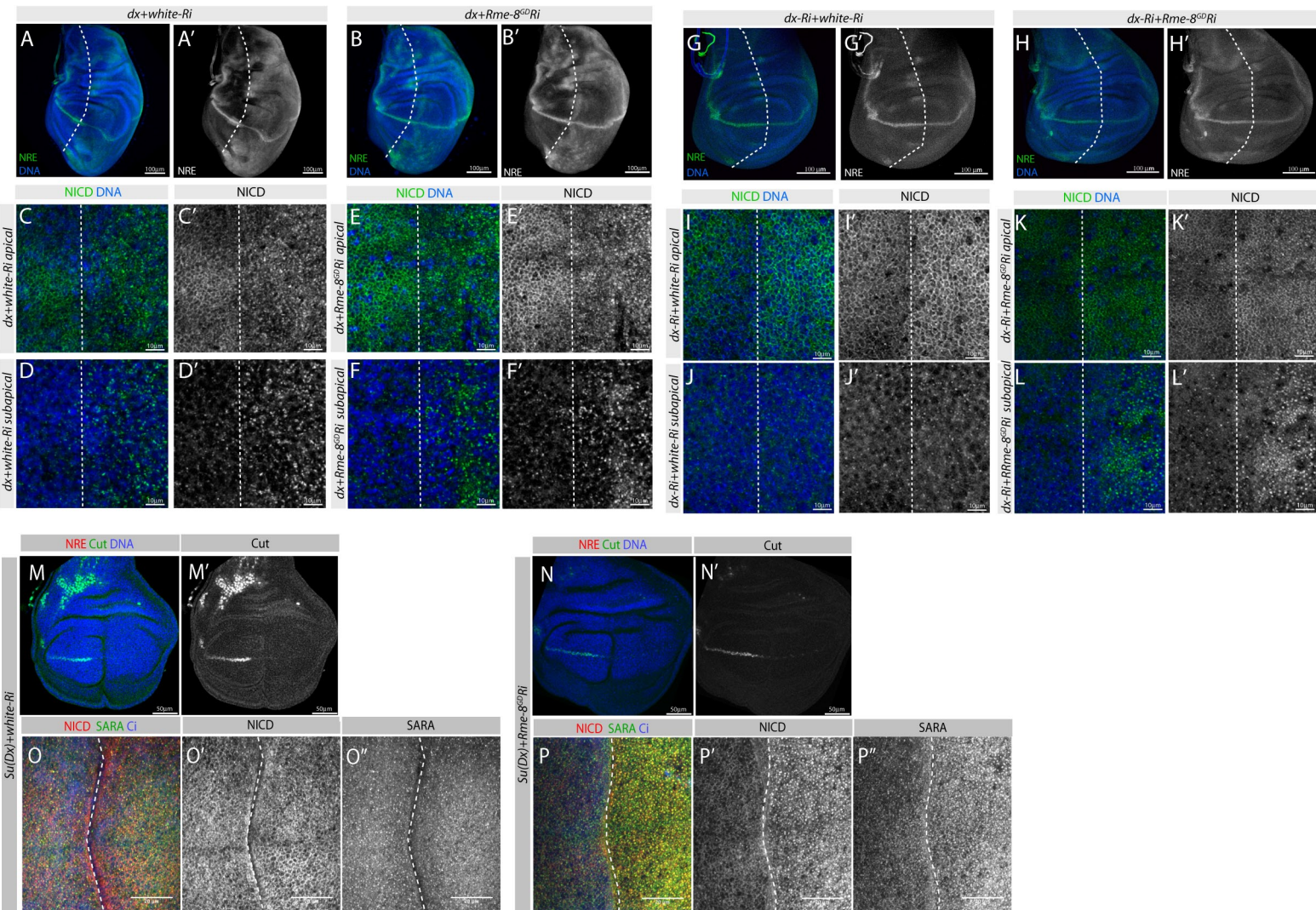
**(C)** *Rme-8<sup>A9</sup>* mutant clones (green) generated by MARCM system show accumulation of intracellular Notch (red in C; white in C').

**(D)** *Rme-8<sup>C19</sup>* mutant clones (green) generated by MARCM system show accumulation of intracellular Wg (red in C; white in C') both inside the receiving cells far from the source of Wg secretion and, to a lesser extent, inside the producing cells.

**(E)** Wing imaginal disc stained for Ci (green), Wg extracellular (red in E; white in E') and Hoescht (blue), shows no difference in Wg extracellular levels in *Rme-8* knock-down cells (right from dotted line).

**(F-G)** Wing imaginal discs stained for Ci (green), Senseless (red in F-G; white in F'-G') and Hoescht (blue), shows no change in Senseless levels of expression in *Rme-8* knock-down cells (right from dotted line in G), compared to  $\frac{1}{2}$  WT (*white-Ri*, right from dotted line in F).

## Gomez-Lamarca, Supplementary Figure 2



### Supplementary Figure 2: *Rme-8* appears regulate Notch trafficking independently of *Dx* and *Su(Dx)*.

**(A-B)** NRE-GFP expression (green in A, B; white in A', B') is detected throughout the domain of *Dx* overexpression (A, right of dotted line) and is not rescued by depletion of *Rme-8* (B, right of dotted line).

**(C-F)** Notch (green, in C-F; white in C'-F') is depleted from the apical membrane and accumulates intracellularly in both *dx* expressing (C, D respectively) and *dx+Rme8-Ri* expressing cells (E, F respectively).

Images are from third instar wing discs expressing either *dx+white-RNAi* (A, C, D) or *dx+Rme8-RNAi* (B, E, F) in the posterior compartment (right of dashed lines).

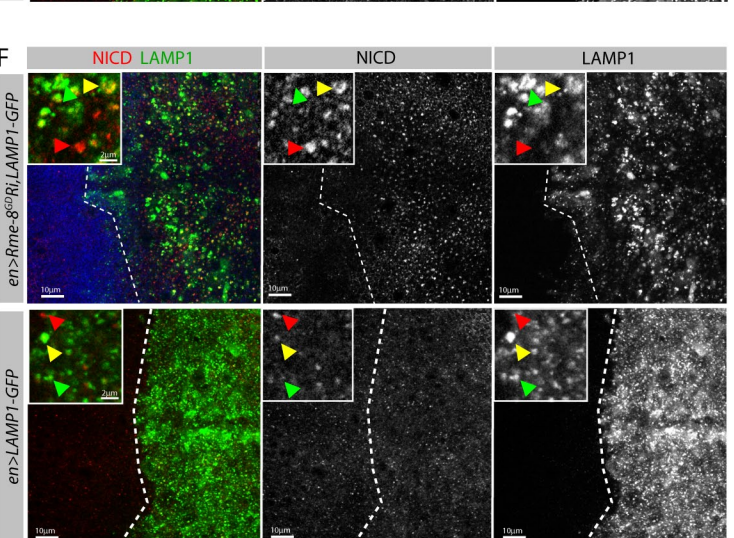
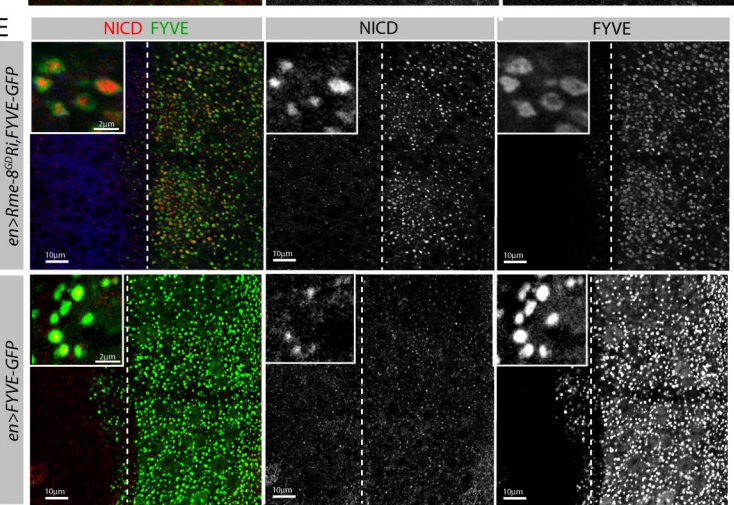
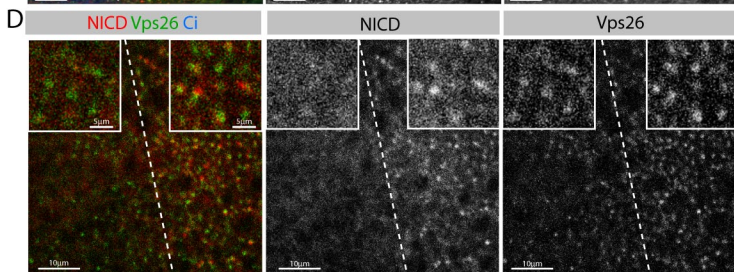
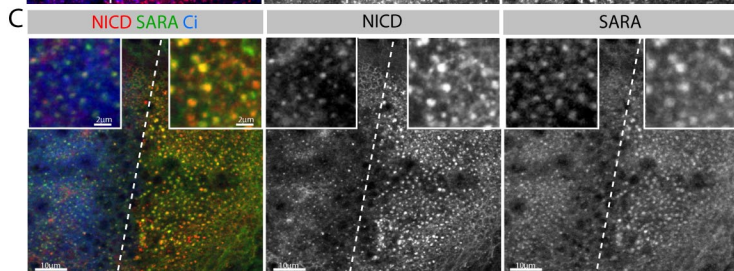
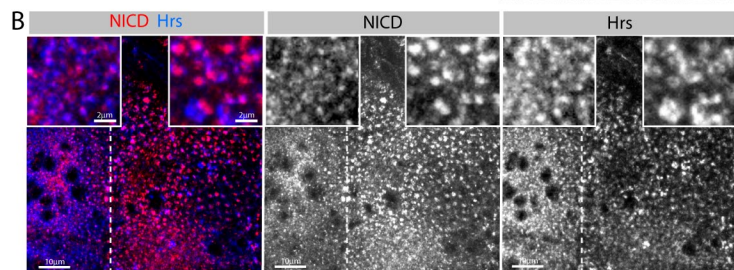
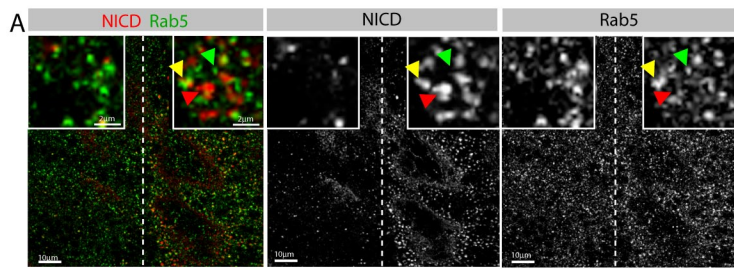
**(G-H)** NRE-GFP expression (green in G, H; white in G', H') is still expressed at the D/V boundary when *dx* is depleted (G, right of dotted line) but is detectably reduced when *Rme-8* is also knocked-down (H, right of dotted line).

**(I-L)** Notch (green, in I-L; white in I'-L') accumulates at the apical membrane in both *dx-Ri* expressing (I, J) and *dx-Ri+Rme8-Ri* expressing cells (K, L) but in subapical endosomes only in *dx-Ri+Rme8-Ri* expressing cells (K, L). Images are from third instar wing discs expressing either *dx-Ri+white-Ri* (G, I, J) or *dx-Ri+Rme8-Ri* (H, K, L) in the posterior compartment (right of dashed lines).

**(M-N)** Cut expression (red in M, N; white in M', N') is depleted at the D/V boundary when *Su(dx)* is overexpressed alone (M, right of dotted line) or in combination with *Rme-8* knockdown (N, right of dotted line).

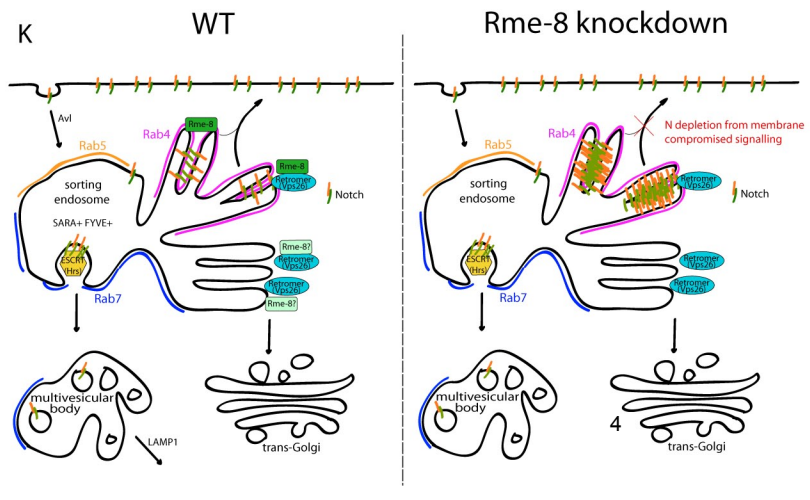
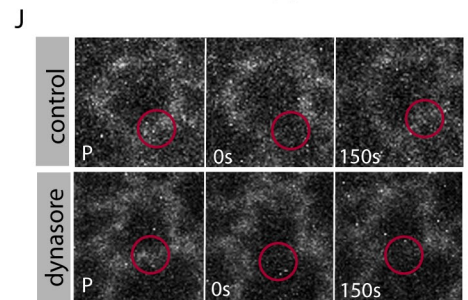
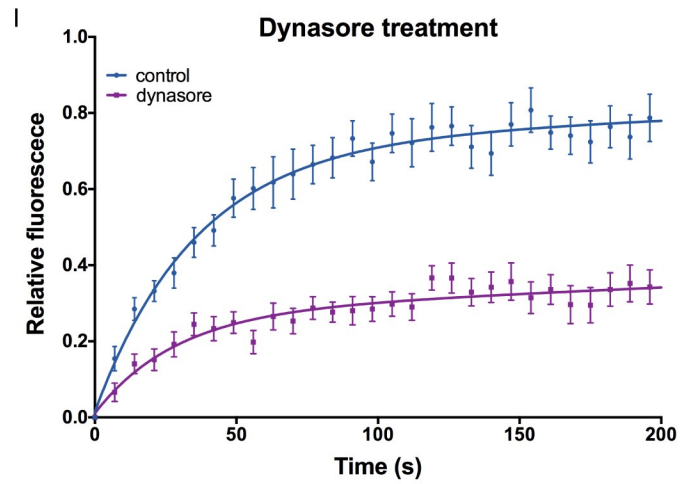
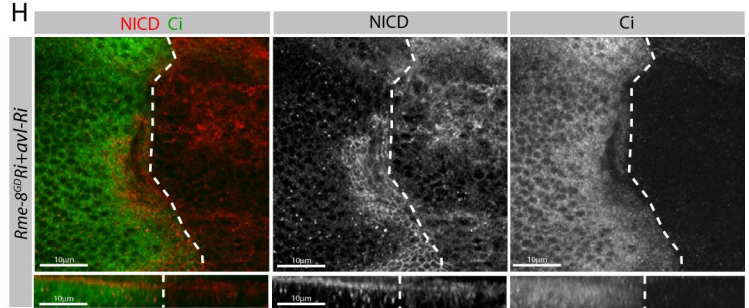
**(O-P)** Distribution of NICD (red in O,P; white in O',P'), SARA (green M,N; white in O'',P'') and Ci (Blue in O,P) from wing discs expressing *Su(Dx)+white-Ri* (O) or *Su(Dx)+Rme-8-Ri* (P) showing that *Rme-8* does not modified *Su(dx)* phenotype.

# Gomez-Lamarca, Supplementary Figure 3



**G**

endosome	marker	changed size	N association
Early	Rab5	NO	adjacent
Recycling	Rab11	YES	adjacent
	Rab4	YES	coincident
Sorting	Vps26	YES	coincident
	FYVE	YES	coincident
	Hrs	YES	adjacent
Mature	SARA	YES	coincident
	Rab7	YES	adjacent
TransGolgi	LAMP1	YES	partially coincident
	Lvl	NO	NO



### Supplementary Figure S3: Notch associates with enlarged endosomes

**(A-D)** Relationship between Notch (NICD) and endocytic proteins in wing discs expressing *Rme8-RNAi* in the posterior compartment (right side of dashed line).

**(A)** Enlarged puncta containing NICD (red) but not Rab5 (green) are detected in the *Rme-8* depleted cells, NICD appears to accumulate away from Rab5 (see insets). **(B)** Enlarged puncta containing NICD (red) and Hrs (blue) are detected in the *Rme-8* depleted cells, NICD appears to accumulate beside Hrs (see insets). **(C)** Enlarged puncta containing NICD (red) and SARA (green) are detected in the *Rme-8* depleted cells; NICD appears to colocalize with SARA (see insets). **(D)** Enlarged puncta containing NICD (red) and Vps26 (red) are detected in the *Rme-8* depleted cells; NICD colocalizes with Vps26 (see insets).

**(E)** Enlarged NICD puncta (red) appear surrounded by FYVE (green). Similar relationship is detected in wild-type tissues, where the puncta are smaller; FYVE-GFP expression alone does substantially alter the Notch accumulations.

**(F)** Enlarged puncta containing NICD (red) and LAMP1 (green) are detected in the *Rme-8* depleted cells. Some puncta contain both proteins (inset, yellow arrowhead) others contain LAMP1 only (inset, green arrowhead) or NICD only (inset, red arrowhead). LAMP1 distribution is also disrupted in comparison to controls (lower panels). Expression of LAMP1-GFP alone does not lead to altered accumulation of NICD.

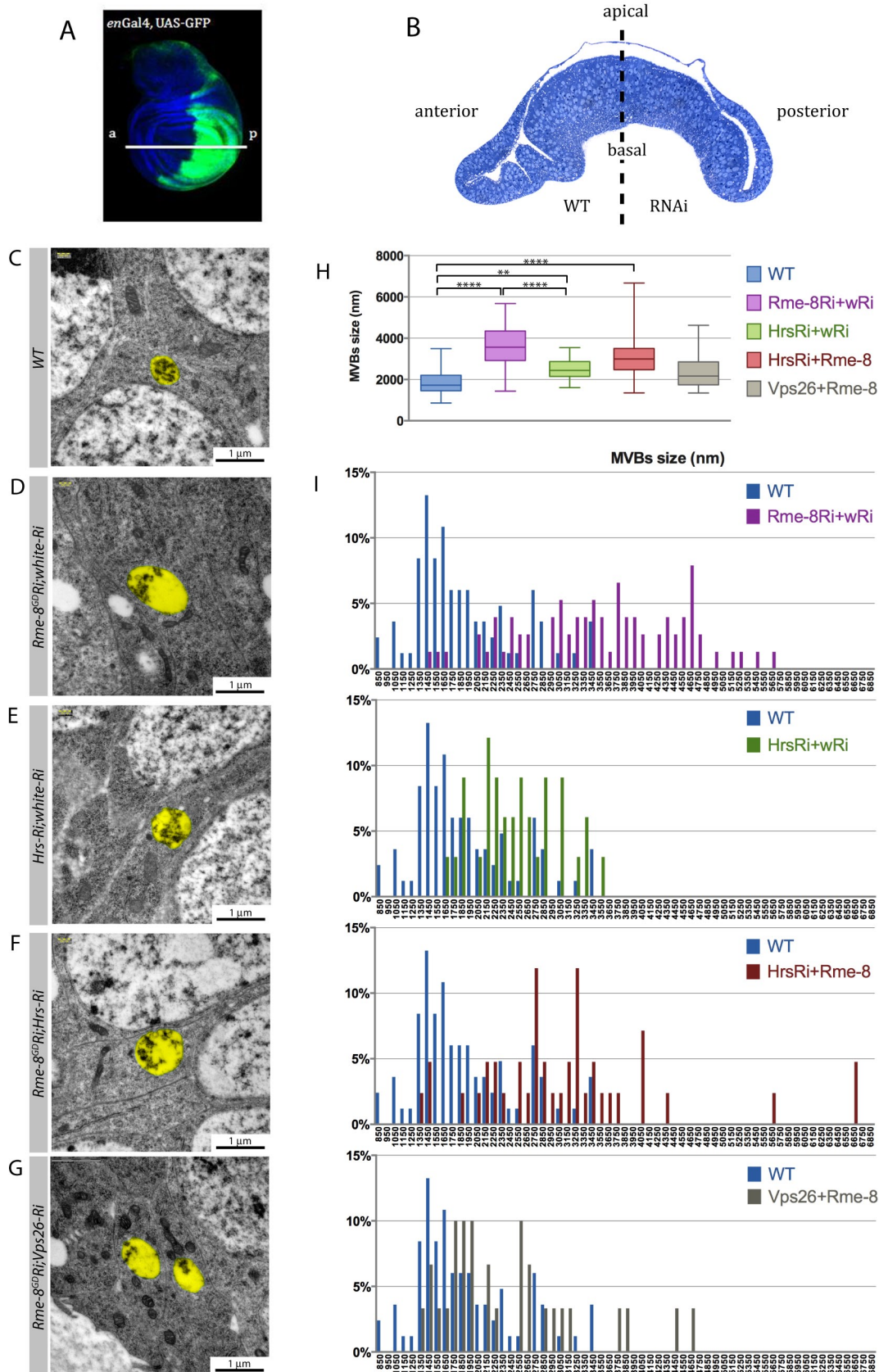
**(G)** Summary table with relevant information about the endosomal markers analysed in *Rme-8* depleted cells.

**(H)** *Avl* knock-down suppresses Notch accumulation in *Rme-8* depleted cells. Distribution of NICD (red in A; white in A') and Ci (green A; white in A'') from wing discs expressing *avl-Ri+Rme-8-Ri*; xy section of discs at the sub-apical plane (upper panel) and xz cross-sections of the same specimens (lower panel).

**(I-J)** FRAP experiments, measuring recovery of Notch-GFP after photo-bleaching. **(I)** Plot of averaged recovery curves (mean  $\pm$  SEM) from Notch-GFP FRAP experiments with best-fit curves as solid lines of WT and dynasore treated discs. **(J)** Single FRAP examples with red circles showing the bleach spots. (P=prebleach).

**(K)** Proposed model of *Rme-8* function in WT and subsequent N trafficking changes in *Rme-8* depleted conditions.

# Gomez-Lamarca, Supplementary Figure 4



## Supplementary Figure 4: TEM analysis of *Rme-8*, *Hrs* and *Vps26* Knockdowns

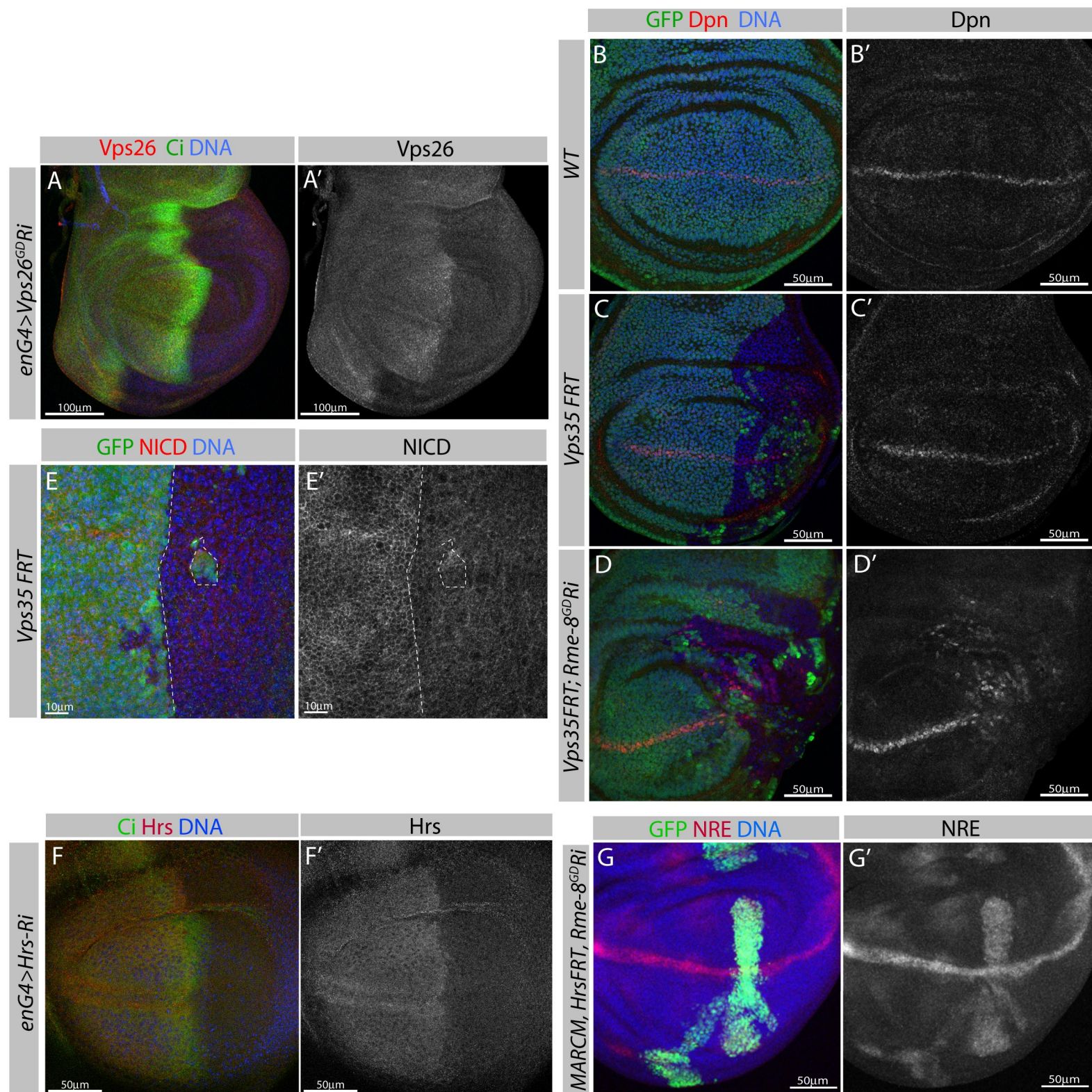
**(A)** Wing disc stained for Hoescht (blue), showing the expression pattern of *en-Gal4* revealed by *UAS-GFP* (green), which was used to express different *UAS RNAi*. The discs were sectioned at the level of the white line.

**(B)** Semi cross-section at the level indicated by the white line in A. Phenotypes of the posterior cells were compared to the anterior wild-type (wt) cells.

**(C-G)** Representative MVBs highlighted in pseudo-colour (yellow) of anterior WT (C), posterior *Rme-8*-depleted (D), *Hrs*-depleted (E), *Rme-8+Hrs*-depleted (F) and *Rme-8+Vps26*-depleted (G) cells. The MVBs of all knockdown conditions are enlarged compared with the control, except those of the *Rme-8+Vps26* double knockdown.

**(H)** Box Plot and statistical analysis of the perimeter of the MVBs. All measurements from anterior compartment MVBs in the four knock-down experiments were included in the WT group for the statistical analysis. Asterisks indicate statistical differences. WT n=83, *Rme-8-Ri;w-Ri* n=76, *Hrs-Ri;w-Ri* n=33, *Hrs-Ri;Rme-8-Ri* n=42, *Vps26-Ri;Rme-8-Ri* n=30<sub>6</sub>

**(I)** Frequency distribution plots of MVB sizes for each condition.



### Supplementary Figure 5: Retromer and ESCRT-0 RNAi validation and phenotypes

**(A)** Wing disc stained for Hoescht (blue), Ci (green) and Vps26 (red) to show the knockdown effect of the *Vps26-Ri* line using *en-Gal4* to direct its expression.

**(B-D)** Wing discs stained for Hoescht (blue) and GFP (green). Dpn expression (red in B-D; white in B'-D') is up-regulated in *Vps35* mutant clones (absence of GFP) expressing *Rme-8Ri* under *hh-Gal4* control (D) compared with WT (A) or *Vps35* mutant alone (B).

**(E)** Wing discs stained for Hoescht (blue) and GFP (green). Membrane levels of Notch (red) are reduced in *Vps35* mutant clones (absence of GFP).

**(F)** Wing disc stained for Hoescht (blue), Ci (green) and Hrs (red) to show the knockdown effect of the *Hrs-Ri* line using *en-Gal4* to direct its expression.

**(G)** NRE-mCherry expression (red in G; white in G') is up-regulated autonomously in *Hrs* mutant clones (GFP+, green) expressing *Rme-8Ri*.

## SUPPLEMENTARY TABLES (ADDITIONAL DETAILS RELATING TO METHODS)

**Table S1: Details of *Drosophila* strains**

<b>Strains</b>	<b>Summary</b>	<b>Reference</b>
<i>Rme-8 Ri GD</i>	322bp hairpin against exon 7	VDRC 22671
<i>Rme-8-Ri KK</i>	768bp hairpin against exon7	VDRC 107706
<i>w-Ri</i>	21bp hairpin against exon 4	BL 35573
<i>Su(H)-Ri</i>	431bp hairpin against exon 3	BL 28900
<i>Dx-Ri GD</i>	338bp hairpin against exon 1	VDRC 7795
<i>Dx-Ri KK</i>	301bp hairpin against exon 2	VDRC 106086
<i>Vps26-Ri</i>	321bp hairpin against exon 2	VDRC 18396
<i>Vps26-Ri</i>	21bp hairpin against exon 2	BL 38937
<i>Hrs-Ri</i>	21bp hairpin against exon 4	BL 33900
<i>Hrs-Ri</i>	21bp hairpin against exon 4	BL 34086
<i>Stam-Ri</i>	361bp hairpin against exon 3	VDRC 22497
<i>KuzDN</i>	dominant-negative construct expressing a version of Kux lacking the metalloprotease domain	BL 6578, Pan and Rubin, 1997
<i>UAS-Dx</i>	full length Deltex cloned in pUAST plasmid	Matsuno et al, 2002
<i>UAS-Su(Dx)</i>	Full open reading frame of Su(Dx) inserted into the pUAST vector	Cornell et al, 1999
<i>SalEPv-Gal4</i>	1080 bp fragment from the sal enhancer (salEPv) clones into pW8-Gal4	Cruz et al, 2009
<i>Rme-8 C19</i>	X-ray mutagenesis	Chang et al, 2004
<i>Rme-8 A9</i>	X-ray mutagenesis	Chang et al, 2004
<i>Vps35 MH20</i>	A 2-Kb deletion that removes the first three exons including the translation start site obtained by P-element imprecise excision	Franch-Marro et al, 2008
<i>Hrs D28</i>	nonsense mutation at amino acid Q270	Lloyd et al, 2002
<i>NRE-Cherry</i>	3 copies of Gbe palindromic binding site plus the Su(H) binding sites from the E(Spl) m8 gene, upstream of the hsp70 minimal promoter controlling the expression of mCherry inserted using the FC31 system	Housden et al, 2012
<i>NRE-GFP</i>	3 copies of Gbe palindromic binding site plus the Su(H) binding sites from the E(Spl) m8 gene, upstream of the hsp70 minimal promoter controlling the expression of eGFP inserted using the FC31 system	Housden et al, 2012
<i>Tub-Rab4-mCherry</i>	construct generated by slice over extension PCR from EST-clone RE40706 (DGRC) and mCherry-cDNA (pAB118-mCherry) and cloned into pCasp-tubPromoter-3'UTR	Yousefian et al, 2013
<i>UAS-GFP-myc-2xFYVE</i>	2 FYVE fingers from Hrs (a.a 147-223) separated by the linker QGQGA and tagged with a myc and eGFP epitope in the N-terminus cloned into pUAST vector	Wucherpfenning et al, 2003
<i>UAS-Lamp1-GFP</i>	cleavable preprolactin signal sequenced followed by eGFP and a transmembrane domain and cytoplasmic tail derived from human LAMP1 cloned into the pUAST vector	BL 42714 Pulipparacharuvil et al, 2005
<i>Notch-GFP</i>	Rescue construct containing 44868 nucleotides from -6.233 nucleotides upstream the transcription start site to 1245 nucleotides downstream of the 3'UTR cloned into attb-P(acman)-ApR vector and a GFP inserted in intracellular domain of Notch (a.a 2388)	Couturier et al, 2012

**Table S2: Details of Primary Antibodies**

Antibody	Dilution	Antigen	Reference
Mo NICD	1/20	Intracellular domain of <i>Drosophila</i> Notch, amino acids 1791-2504	C17.9C6 DSHB, Fehon et al, 1990
Mo NECD	1/20	EGF repeats 12-20 of the extracellular domain of <i>Drosophila</i> Notch	C458.2H DSHB Diederich et al, 1994
Rat NECD	1/500	Extracellular domain of <i>Drosophila</i> Notch	Fehon et al, 1990
Mo Wg	1/20	Wg amino acids 3-468 fused to TrpE	4E4 DSHB, Heuvel et al, 1989
GP DI	1/3000	EGF-like repeats 4- 9, amino acids 350-529, of <i>Drosophila</i> Delta fused to b-Galactosides	Huppert et al, 1997
Rat Ci	1/20	amino-acids 700-850 (C-terminus of the Zn finger domain) of Ci fused to glutathione-S-transferase	2A1 DSHB, Motzny and Holmgren, 1995
Rb GFP	1/1000	Polyclonal against GFP isolated directly from jellyfish <i>Aequorea victoria</i>	A6455 invitrogen
Rb dsRed	1/200	polyclonal	632496 Clontech
Rb Rab7	1/3000	Synthetic peptide CNDFPDQITLGSQNNRPG, amino acid residues 184-200 of <i>Drosophila</i> Rab7	Tanaka and Nakamura, 2008
Rb Rab11	1/8000	Synthetic peptide CSQKQIRDPEGDVI, amino acid residues 177-191 of <i>Drosophila</i> Rab11	Tanaka and Nakamura, 2008
Rb Rab5	1/500	Synthetic peptide covering amino-acids 200 to C-terminus of Rab5 fused to KLH	31261 abcam
GP Hrs	1/1000	N-terminal domain of HRS fused to GST	Lloyd et al, 2002
Rb Lva	1/500	Fragment close to the C-terminus domain of Lavalamp fused to GST	Sisson et al, 2000
Rb Avl	1/1000	Peptide covering amino acids 1-258 from <i>avl</i> cDNA fused to GST	Lu and Bilder, 2005 Coumilleau et al, 2009
Rb SARA	1/500	C-terminal 174 amino acids fused to GST	
GP Vps26	1/1000	Full length Vps26 protein fused to Hisx6	Wang et al, 2014

Mo=Mouse; GP=Guinea- pig; Rb=Rabbit;

**Table S3: Details of Secondary Antibodies**

Antibody	Specificity	Catalogue number
Donkey anti-Mo FITC	AffiniPure Donkey anti-Mouse IgG (H+L)	715-095-151 Jackson ImmunoResearch
Donkey anti-Mo Cy3	AffiniPure Donkey anti-Mouse IgG (H+L)	715-165-151 Jackson ImmunoResearch
Donkey anti-Mo Cy5	AffiniPure Donkey anti-Mouse IgG (H+L)	715-175-151 Jackson ImmunoResearch
Donkey anti-Mo 488	Donkey anti-Mouse IgG (H+L)	A21202 Invitrogen
Donkey anti-Rb FITC	AffiniPure Donkey anti-Rabbit IgG (H+L)	711-095-152 Jackson ImmunoResearch
Goat anti-Rb Cy3	AffiniPure Goat anti-Rabbit IgG (H+L)	111-165-144 Jackson ImmunoResearch
Donkey anti-Rb Cy5	AffiniPure Donkey anti-Rabbit IgG (H+L)	711-175-152 Jackson ImmunoResearch
Donkey anti-Rb 568	Donkey anti-Rabbit IgG (H+L)	A10042 Invitrogen
Donkey anti-Rat FITC	AffiniPure Donkey anti-Rat igG (H+L)	712-095-153 Jackson ImmunoResearch
Donkey anti-Rat Cy3	AffiniPure Donkey anti-Rat igG (H+L)	712-165-153 Jackson ImmunoResearch
Donkey anti-Rat Cy5	AffiniPure Donkey anti-Rat igG (H+L)	712-175-153 Jackson ImmunoResearch
Donkey anti-GP FITC	AffiniPure Donkey anti-Guinea Pig IgG (H+L)	706-095-148 Jackson ImmunoResearch
Donkey anti-GP Cy3	AffiniPure Donkey anti-Guinea Pig IgG (H+L)	706-165-148 Jackson ImmunoResearch

Mo=Mouse; GP=Guinea- pig; Rb=Rabbit;

## SUPPLEMENTARY REFERENCES

- Chang, H.C., M. Hull, and I. Mellman. 2004. The J-domain protein Rme-8 interacts with Hsc70 to control clathrin-dependent endocytosis in *Drosophila*. *The Journal of Cell Biology*. 164:1055-1064.
- Cornell, M., D.A. Evans, R. Mann, M. Fostier, M. Flasza, M. Monthatong, S. Artavanis-Tsakonas, and M. Baron. 1999. The *Drosophila melanogaster* Suppressor of deltex gene, a regulator of the Notch receptor signaling pathway, is an E3 class ubiquitin ligase. *Genetics*. 152:567-576.
- Coumailleau, F., M. Fürthauer, J.A. Knoblich, and M. González-Gaitán. 2009. Directional Delta and Notch trafficking in Sara endosomes during asymmetric cell division. *Nature*. 458:1051-1055.
- Couturier, L., K. Mazouni, and F. Schweisguth. 2013. Numb localizes at endosomes and controls the endosomal sorting of notch after asymmetric division in *Drosophila*. *Current biology : CB*. 23:588-593.
- Cruz, C., A. Glavic, M. Casado, and J.F. de Celis. 2009. A Gain-of-Function Screen Identifying Genes Required for Growth and Pattern Formation of the *Drosophila melanogaster* Wing. *Genetics*. 183:1005-1026.
- Diederich, R.J., K. Matsuno, H. Hing, and S. Artavanis-Tsakonas. 1994. Cytosolic interaction between deltex and Notch ankyrin repeats implicates deltex in the Notch signaling pathway. *Development*. 120:473-81.
- Fehon, R.G., P.J. Kooh, I. Rebay, C.L. Regan, T. Xu, M.A.T. Muskavitch, and S. Artavanis-Tsakonas. 1990. Molecular interactions between the protein products of the neurogenic loci Notch and Delta, two EGF-homologous genes in *Drosophila*. *Cell*. 61:523-534.
- Franch-Marro, X., F. Wendler, S. Guidato, J. Griffith, A. Baena-Lopez, N. Itasaki, M.M. Maurice, and J.-P. Vincent. 2008. Wingless secretion requires endosome-to-Golgi retrieval of Wntless/Evi/Sprinter by the retromer complex. *Nature Cell Biology*. 10:170-177.
- Housden, B.E., K. Millen, S.J. Bray, and B.J. Andrews. 2012. *Drosophila* Reporter Vectors Compatible with  $\Phi$ C31 Integrase Transgenesis Techniques and Their Use to Generate New Notch Reporter Fly Lines. *G3 (Bethesda, Md.)*. 2:79-82.
- Huppert, S.S., T.L. Jacobsen, and M.A. Muskavitch. 1997. Feedback regulation is central to Delta-Notch signalling required for *Drosophila* wing vein morphogenesis. *Development*. 124:3283-3291.
- Lloyd, T.E., R. Atkinson, M.N. Wu, Y. Zhou, G. Pennetta, and H.J. Bellen. 2002. Hrs regulates endosome membrane invagination and tyrosine kinase receptor signaling in *Drosophila*. *Cell*. 108:261-269.
- Lu, H., and D. Bilder. 2005. Endocytic control of epithelial polarity and proliferation in *Drosophila*. *Nature Cell Biology*. 7:1232-1239.
- Matsuno, K., M. Ito, K. Hori, F. Miyashita, S. Suzuki, N. Kishi, S. Artavanis-Tsakonas, and H. Okano. 2002. Involvement of a proline-rich motif and RING-H2 finger of Deltex in the regulation of Notch signaling. *Development*. 129:1049-1059.
- Motzny, C.K., and R. Holmgren. 1995. The *Drosophila cubitus interruptus* protein and its role in the wingless and hedgehog signal transduction pathways. *Mech Dev*. 52:137-50.
- Pan, D., and G.M. Rubin. 1997. Kuzbanian controls proteolytic processing of Notch and mediates lateral inhibition during *Drosophila* and vertebrate neurogenesis. *Cell*. 90:271-80.
- Pulipparacharuvil, S., M.A. Akbar, S. Ray, E.A. Sevrioukov, A.S. Haberman, J. Rohrer, and H. Kramer. 2005. *Drosophila* Vps16A is required for trafficking to lysosomes and biogenesis of pigment granules. *J Cell Sci*. 118:3663-73.
- Sisson, J.C., C. Field, R. Ventura, A. Royou, and W. Sullivan. 2000. Lava lamp, a novel peripheral golgi protein, is required for *Drosophila melanogaster* cellularization. *The Journal of Cell Biology*. 151:905-918.
- Tanaka, T., and A. Nakamura. 2008. The endocytic pathway acts downstream of Oskar in *Drosophila* germ plasm assembly. *Development*. 135:1107-1117.
- van den Heuvel, M., R. Nusse, P. Johnston, and P.A. Lawrence. 1989. Distribution of the wingless gene product in *Drosophila* embryos: a protein involved in cell-cell communication. *Cell*. 59:739-49.
- Wang, S., K.L. Tan, M.A. Agosto, B. Xiong, S. Yamamoto, H. Sandoval, M. Jaiswal, V. Bayat, K. Zhang, W.-L. Charng, G. David, L. Duraine, K. Venkatachalam, T.G. Wensel, and H.J. Bellen. 2014. The Retromer Complex Is Required for Rhodopsin Recycling and Its Loss Leads to Photoreceptor Degeneration. *PLoS Biology*. 12:e1001847.
- Wucherpennig, T., M. Wilsch-Bräuninger, and M. González-Gaitán. 2003. Role of *Drosophila* Rab5 during endosomal trafficking at the synapse and evoked neurotransmitter release. *The Journal of Cell Biology*. 161:609-624.
- Yousefian, J., T. Troost, F. Grawe, T. Sasamura, M. Fortini, and T. Klein. 2013. Dmon1 controls recruitment of Rab7 to maturing endosomes in *Drosophila*. *Journal of cell science*. 126:1583-1594.